Effect of metal oxides on zirconia for ketonic decarboxylation of methyl stearate

Miss Pawaphat Sartsri

A Thesis Submitted in Partial Fulfillment of the Requirements

for the Degree of Master of Engineering in Chemical Engineering

Department of Chemical Engineering

Faculty of Engineering

Chulalongkorn University

Academic Year 2018

ผลของโลหะออกไซด์บนเซอร์โคเนียสำหรับปฏิกิริยาคีโตนิกดีคาร์บอกซิเลชันของเมทิลสเตียเรท

น.ส.ภาวภัทร ศาสตร์ศรี

จุฬาลงกรณ์มหาวิทยาลัย

CHULALONGKORN UNIVERSITY

วิทยานิพนธ์นี้เป็นส่วนหนึ่งของการศึกษาตามหลักสูตรปริญญาวิศวกรรมศาสตรมหาบัณฑิต
สาขาวิชาวิศวกรรมเคมี ภาควิชาวิศวกรรมเคมี
คณะวิศวกรรมศาสตร์ จุฬาลงกรณ์มหาวิทยาลัย
ปีการศึกษา 2561

Thesis Title   Effect of metal oxides on zirconia for ketonic

decarboxylation of methyl stearate

By   Miss Pawaphat Sartsri

Field of Study   Chemical Engineering

Thesis Advisor   Professor PIYASAN PRASERTHDAM, Dr.Ing.

Accepted by the Faculty of Engineering, Chulalongkorn University in Partial Fulfillment of the Requirement for the Master of Engineering

                              Dean of the Faculty of Engineering

(Professor SUPOT TEACHAVORASINSKUN, D.Eng.)

THESIS COMMITTEE

                              Chairman

(Associate Professor KASIDIT NOOTONG, Ph.D.)

                              Thesis Advisor

(Professor PIYASAN PRASERTHDAM, Dr.Ing.)

                              Examiner

(Professor ARTIWAN SHOTIPRUK, Ph.D.)

                              External Examiner

(Nilubon Jonganurakkun, Ph.D.)

ภวภัทร ศาสตร์ศรี : ผลของโลหะออกไซด์บนเซอร์โคเนียสำหรับปฏิกิริยาคีโตนิกดีคาร์บอกซิเลชันของเมทิลสเตียเรท. (Effect of metal oxides on zirconia for ketonic decarboxylation of methyl stearate) อ.ที่ปรึกษาหลัก : ศ. ดร.ปิยะสาร ประเสริฐธรรม

ในงานวิจัยนี้ศึกษาผลของคุณลักษณะของตัวเร่งปฏิกิริยาเซอร์โคเนียและโลหะออกไซด์บนเซอร์โคเนียที่มีผลต่อปฏิกิริยาคีโตนิกดีคาร์บอกซิเลชันของเมทิลสเตียเรทเพื่อเปลี่ยนเป็นสารผลิตภัณฑ์ประเภทคีโตน โดยทำการทดลองที่อุณหภูมิ ๔๐๐ องศาเซลเซียสภายใต้ความดันบรรยากาศ คุณลักษณะของตัวเร่งปฏิกิริยาเซอร์โคเนียและโลหะออกไซด์บนเซอร์โคเนียสามารถวิเคราะห์โดยใช้เทคนิคการเลี้ยวเบนของรังสีเอ็กซ์ การใช้กล้องจุลทรรศน์อิเล็กตรอนแบบส่องกราด การดูดซับทางกายภาพของไนโตรเจน การใช้เทคนิคเอกซ์เรย์โฟโตอิเล็กตรอนสเปกโตรสโคปี และเทคนิคอินฟาเรดสเปคโตรสโคปีด้วยไพริดีน จากผลการทดลองแสดงให้เห็นว่าการเติมโลหะออกไซด์กลุ่มโลหะแทรนซิชันลงบนตัวเร่งปฏิกิริยาเซอร์โคเนียนั้นมีปริมาณของกรดลิวอิสและช่องว่างของออกซิเจนมากกว่าตัวเร่งปฏิกิริยาตัวอื่นๆ อีกทั้งยังมีกรดบรอนสเตดอยู่ในปริมาณที่น้อย จึงส่งผลให้ผลของการเกิดปฏิกิริยาคีโตนิกดีคาร์บอกซิเลชันของเมทิลสเตียเรทเพิ่มสูงขึ้นรวมไปถึงค่าการเลือกเกิดเป็นสารผลิตภัณฑ์เพิ่มขึ้นอีกด้วย เมื่อทำการเปรียบเทียบผลของคุณลักษณะของตัวเร่งปฏิกิริยาพบว่า ปริมาณของกรดลิวอิสที่อยู่บนพื้นผิวของตัวเร่งปฏิกิริยานั้นส่งผลต่อการเกิดปฏิกิริยา ส่วนช่องว่างของออกซิเจนและปริมาณของกรดบรอนสเตดบนพื้นผิวของตัวเร่งปฏิกิริยาจะส่งผลต่อการเลือกเกิดเป็นสารผลิตภัณฑ์ โดยที่กรดบรอนสเตดมีบทบาทต่อการเลือกเกิดเป็นสารผลิตภัณฑ์มากกว่าช่องว่างของออกซิเจน

สาขาวิชา	วิศวกรรมเคมี	ลายมือชื่อนิสิต ....
ปีการศึกษา	2561	ลายมือชื่อ อ.ที่ปรึกษาหลัก ....

6070270221 : MAJOR CHEMICAL ENGINEERING

KEYWORD: KETONIC DECARBOXYLATION, ACIDITY, OXYGEN VACANCIES, ZIRCONIA

Pawaphat Sartsri : Effect of metal oxides on zirconia for ketonic decarboxylation of methyl stearate . Advisor: Prof. PIYASAN PRASERTHDAM, Dr.Ing.

In this research, the effect of characteristics of zirconia and metal oxide modified zirconia catalysts on the catalytic performance were investigated by ketonic decarboxylation of methyl stearate to desired ketone product at the optimal condition (400°C and 1 bar). Zirconia and metal oxide modified zirconia catalysts were characterized by using X-ray diffraction (XRD), Scanning electron microscope (SEM), N_2-physissorption, X-ray photoelectron spectroscopy (XPS), and IR spectra of pyridine adsorption (Pyridine-IR). The results indicated that the transition metal oxide group modified zirconia catalysts have higher contents of total Lewis acid site and oxygen vacancies site, and lower content of total Brønsted acid site on the surface of catalysts, which provides high conversion and high selectivity. For the comparison of the Lewis and Brønsted acid site,and oxygen vacancies site, it can be concluded that the conversion of methyl stearate only depends on Lewis acid site. Furthermore, Brønsted acid site affecting selectivity as well as oxygen vacancies site, but the Brønsted acid site plays an important role in the selectivity of desired ketone product more than the oxygen vacancies site.

Field of Study:	Chemical Engineering	Student's Signature	....
Academic Year:	2018	Advisor's Signature	....

ACKNOWLEDGEMENTS

TABLE OF CONTENTS

LIST OF TABLES

จุฬาลงกรณ์มหาวิทยาลัย
CHULALONGKORN UNIVERSITY

LIST OF FIGURES

CHAPTER I

INTRODUCTION

1.1 Introduction

Due to the limited reserves of fossil fuels, increasing the environmental concerns, and the depletion of the world's petroleum reserves, many researchers have found a new energy resource that is renewable, reliable, clean and yet economically available as a substitution to the fossil fuels. Biodiesel described as an alternative fuel composed of mono-alkyl esters of long-chain fatty acids derived from non-edible vegetable oil has been noted to be a viable alternative to the conventional transport fuel, petro-diesel for diesel engines and is earning worldwide attention [1]. Biodiesel is better than diesel fuel because it can be utilized in any compression ignition engine without the need for modification, its nontoxicity in terms of sulfur content, aromatic content, and carbon neutrality, renewability, and biodegradability [2].

In recent years, Thailand is the third largest producer of palm oil. Palm oil is important in terms of food security and as global energy. Thanks to its tropical climate, the country can produce significant amounts of oil palm, as global demand for it increases. Thailand has more than 200,000 small-scale palm oil farmers who make up much of the industry, and it has seen an increase in areas for palm oil production over the years. That explains why the costs of producing palm oil in Thailand are higher than in Malaysia and Indonesia, where palm oil growing is a big agricultural industry.

Figure 1 Palm oils are harvest in Thailand[3].

The main problem is the effort to expand the market fails, the increase of plantation areas may lead to oversupply, and prices will stay low couples with the export markets overseas are rather saturated now. The demand for palm oil will become greater if those sectors want more. Palm oil is mainly used in consumer goods such as soap and cosmetics and in food industries. For biodiesel, it depends on the government strategy on energy. There are not many engines consume biodiesel in Thailand so there is not a large amount of demand for palm oil in this sector. Although local output is down while the demand remains unchanged, there continues to be an overstock of palm oil cause an oversupply of biodiesel [3].

The increasing focus on promoting the use of biodiesel more in various applications. Therefore, the transformation of biomass conversion to other valued products was increased constantly in industry and academia. Apart from fuels and polymers, another classical type of petroleum-derived products is waxes [4]. Ketonic decarboxylation is an important approach for carboxylic acid upgrading. María Jesús Ramos *et al.* (2014) were studied the influence of fatty acid composition of raw materials on biodiesel properties. There are fatty acids were identified in the palm oil biodiesel as shown in Table 1 that can be present in a triglyceride including saturated (Cn:0), monounsaturated (Cn:1) and polyunsaturated with two or three double bonds (Cn:2) or (Cn:3).

Table 1 Fatty acid profiles (wt.%) of palm oil biodiesel [5]

Fatty acid		wt.%
Lauric	C12:0	0.1
Myristic	C14:0	0.7
Palmitic	C16:0	36.7
Palmitoleic	C16:1	0.1
Stearic	C18:0	6.6
Oleic	C18:1	46.1
Linoleic	C18:2	8.6
Linolenic	C18:3	0.3
Arachidic	C20:0	0.4
Gadoleic	C20:1	0.2
Behenic	C22:0	0.1
Erucic	C22:1	0.0
Lignoceric	C24:0	0.1
Nervonic	C24:1	0.0

Currently, the ketonic decarboxylation of carboxylic acids has been studied with the aim to produce fuels from fatty acids. The reaction pathway is explained in Figure 2.
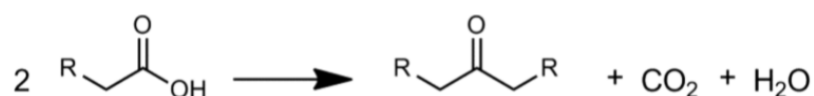
Figure 2 Reaction pathway for the ketonic decarboxylation of carboxylic acids [4].

Ketonic decarboxylation fits very well as in this reaction of carboxylic acids. It converts two carboxylic acids into ketones forming one carbon–carbon bond and eliminates three oxygen atoms as carbon dioxide and water [6]. The reaction can also be applied directly to esters, but these compounds have less interest to produce esters since the selectivity to the ketone observed were lower than for the carboxylic

acids. Furthermore, hydrocarbons and shorter ketones were obtained as byproducts when using the esters [4]. Therefore, it is a big challenge to use methyl stearate (C18:0), which one of the esters in Fatty Acid Methyl Esters (FAME) in biodiesel as raw material instead of fatty acids because it not widely uses a high number of hydrocarbon ester for ketonic decarboxylation. This ester may or may not be useful as a source for the ketone production, but it may find application for other purposes. Therefore, more research is needed to explore its potentials for future industrial. In general, the process can be carried out in a continuous flow reactor at temperatures in the range of 350-400 °C, and monoclinic zirconia has been shown as a very suitable catalyst for this reaction [7, 8].

The aims of this work are to present a study of the ketonic decarboxylation of ester, methyl stearate, in the gas phase over heterogeneous catalysts and improve the catalytic activity for this reaction. The modified metal oxide supported on zirconia catalysts have been investigated. Such studies would enable a comparison of the characteristics of catalysts. The significant roles of catalytic properties influence catalytic activity and selectivity of this ketonic decarboxylation reaction. Besides, the catalysts were characterized by various techniques and correlated to the catalytic performance in ketonic decarboxylation for easily choosing the most active ones.

1.2 Objective

To investigate the effect of oxygen vacancies and acidity of ZrO_2 and metal oxide modified ZrO_2 catalysts in ketonic decarboxylation of methyl stearate at the optimal condition.

1.3 The scopes of research

1.3.1 The effects of a temperature range of 400-500°C and a pressure range of 1-20 bar of methyl stearate via ketonic decarboxylation reaction were investigated to optimize for finding the optimal condition for operating this reaction and minimizing the cracking reaction by using commercial zirconia (ZrO_2) catalyst.

1.3.2 The samples of metal oxide modified ZrO_2 catalysts were prepared by the incipient wetness impregnation method of a ZrO_2 sample and compered about the characteristics and catalyst properties.

1.3.3 Catalytic performance of this ketonic decarboxylation were tested at the optimal condition over ZrO_2 and metal oxide modified ZrO_2 catalysts.

1.3.4 The desired and undesired products were analyzed off-line by gas chromatography on GC apparatus equipped with flame ionization detector (FID).

1.3.5 The catalysts were characterized by various techniques, as follows:

1) X-ray diffraction (XRD) for analyzing the crystalline structure.

2) Scan electron microscope (SEM) for analyzing the surface topography and metal dispersion.

3) N_2-physisorption for analyzing the surface area.

4) X-ray photoelectron spectroscopy (XPS) for analyzing the binding energy of oxygen vacancy (O1s)

5) IR spectra of pyridine adsorption (Pyridine-IR) for investigating the amount of total Lewis and Brønsted acid site.

1.4 Research methodology

Prepared metal oxide modified ZrO_2 catalysts

by incipient wetness impregnation technique

(Catalysts: 10%CeO_2/ZrO_2, 10%Y_2O_3/ZrO_2, 10%La_2O_3/ZrO_2, 10%MgO/ZrO_2,

and 10%BaO/ZrO_2)

Mixed the powder of the oxide support with redistilled water and

stirred slurry until homogeneous (2 h) and Calcined at 800°C for 3 h in air.

Crushed and sieved fractions of 0.4-0.8 mm

Loading of 10 wt.% metal oxide via incipient wetness impregnation method

Calcined at 450°C for 3 h in air.

Characterizations by
- XRD
- SEM-EDX
- N_2-physisorption
- XPS
- Pyridine-IR

Catalytic testing in ketonic

decarboxylation:
- Temperature = 400 - 500 °C
- Pressure = 1- 20 bar

Discussion

Conclusion

CHAPTER II

BACKGROUND AND LITERATURE REVIEWS

The purpose of this chapter provides the fundamental concept and literature review for this research. The first section of the chapter describes the information of feedstock and desired product. Next section describes of the fundamental information and mechanism about ketonic decarboxylation reaction. Finally, catalysts and literature reviews of this research are explained below:

2.1 Methyl stearate

Methyl stearate is present as a constituent of biodiesel having high number of hydrocarbons. Methyl stearate has an IUPAC name of methyl octadecanoate and it can be called in the other name as Octadecanoic acid, methyl ester or Stearic acid methyl ester. The chemical formula of methyl stearate is $C_{19}H_{38}O_2$ [9]. Methyl stearate is an ester. Esters react with acids to liberate heat along with alcohols and acids. Strong oxidizing acids may cause a vigorous reaction that is sufficiently exothermic to ignite the reaction products. Heat is also generated by the interaction of esters with caustic solutions. Flammable hydrogen is generated by mixing esters with alkali metals and hydrides. The useful of methyl stearate is used as a non-ionic surfactant in various experiments in helping solubilize a variety of chemical species by dissociating aggregates and unfolding proteins [10]. The chemical structure of methyl stearate is shown in Figure 3.
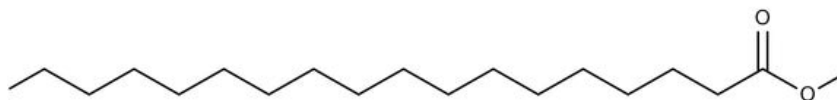
Figure 3 Chemical structure of methyl stearate [10]

Table 2 shows physical and chemical properties of methyl stearate which are important to apply for the industries or experiments.

Table 2 Physical and chemical properties of methyl stearate [9]

Properties	Values
Formula	$C_{19}H_{38}O_2$
Formula Weight	298.511 g/mol
Form	Crystal
Color	White
Melting point	39.1℃
Boiling point	181-182 ℃
Density	0.8498 (rough estimate)
Solubility	Soluble in alcohol, ether or chloroform
Price/unit	79 USD/ 1kg

2.2 18-pentatriacontanone

18-pentatriacontanone has an IUPAC name of pentatriacontan-18-one and it can be called in the other name as Stearone, Stearyl ketone, or Diheptadecyl ketone. The chemical formula of 18-pentatriacontanone is $C_{35}H_{70}O$. This ketone product, 18-pentatriacontanone, is an organic compound with the structure $C_{17}(C=O)C_{17}$ that contain a carbonyl group (a carbon-oxygen double bond) [11], which are shown in Figure 4.
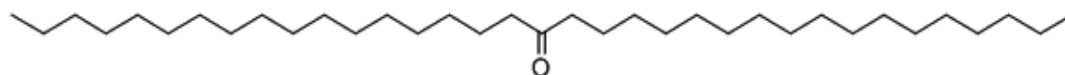
Figure 4 Chemical structure of 18-pentatriacontanone [11]

Table 3 shows physical and chemical properties of 18-pentatriacontanone which are important to apply for the industries or experiments.

Table 3 Physical and chemical properties of 18-pentatriacontanone [12]

Properties	Values
Formula	$C_{35}H_{70}O$
Formula Weight	506.94 g/mol
Form	Powder
Color	Off-white
Melting point	86-87°C
Boiling point	345°C/12 mmHg
Density	0.8635 (rough estimate)
Solubility	Soluble in benzene
Storage & Sensitivity	Ambient temperatures. Store in cool, dry place in tightly closed containers.
Price/unit	200 USD/ 25g

Stearone is also useful, shown in Figure 5. There are many applications of 18-pentatriacontanone. It has many recorded uses as an anti-blocking agent that worked into the film material in small amounts (less than 0.5 wt.%) for minimizing friction between films, an intermediate for preparation of barium derivatives for using in lubricants, pharmaceutical intermediate in term of the building blocks used in the production of active pharmaceutical ingredients, and chemical research such as solvents, and polymer precursors [13].

Figure 5 Applications of 18-pentatriacontanone [12]

2.3 Ketonic Decarboxylation reaction

The ketonic decarboxylation of carboxylic acids by decarboxylation, also called "ketonic decarboxylation", is beneficial synthetically for the production of symmetrical ketones [14]. The basis for this transformation of the ketonic decarboxylation when starting with carboxylic acids is possible to join two molecules of carboxylic acid (with n carbon atoms) by carbon-carbon bond formation to obtain a linear molecule of carbonyl group with 2n-1 carbon atoms, carbon dioxide, and water as innocuous by-products, as follows:

$$R_1COOH + R_2COOH \longrightarrow R_1COR_2 + CO_2 + H_2O$$
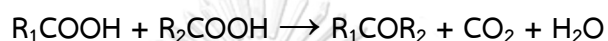
For, ketonic decarboxylation can play a significant role in several biomass conversion processes since it can eliminate the highly reactive carboxylic functional groups while increasing the size of the carbon chain [15] in the presence of metal oxides. This process is considered to be environmentally friendly because non-polluting by-products are produced [16]. Ketonic decarboxylation has been mainly studied using shorter carboxylic acids, such as valeric acid and pentanoic acid.

In general, the process can be carried out in a fixed bed continuous flow reactor over heterogeneous catalysts with the suitable ketonic decarboxylation conditions may include a temperature in the range of 300-500 °C [4, 14, 16-18], and a pressure from atmospheric pressure to 13 bar [17]. This reaction can also be referred directly to esters, but these compounds have not widely credit to produce esters since the selectivity's ketone discovered were lower than the carboxylic acids. Besides, hydrocarbons and shorter ketones were received as byproducts when using the esters [4].

However, long-chain esters can also be considered as a substrate. Methyl stearate can also be applied here for producing long-chain ketones with 31–35 carbon atoms, as described in the equation below:

$$2 \ CH_3(CH_2)_{15}CH_2\overset{O}{\underset{}{C}}OCH_3 \longrightarrow CH_3(CH_2)_{16}\overset{O}{\underset{}{C}}(CH_2)_{16}CH_3 + CO_2 + CH_3OCH_3$$

Methyl stearate   18-pentatriacontanone   Dimethyl ether
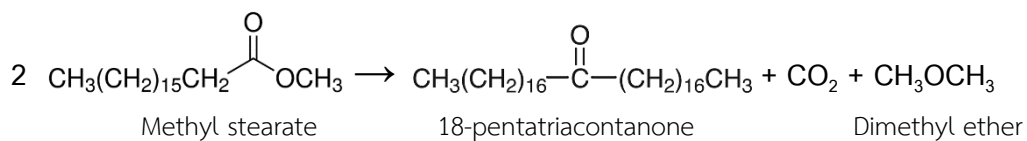
The mainly ketone product, 18-pentatriacontanone or stearone, was obtained. Thereby, carbon dioxide and dimethyl ether are produced, which were not condensed in the liquid phase with our experimental setup. Depending on the temperature, ketonic decarboxylation of the methyl ester fraction produced a liquid or semiliquid mixture of ketones and hydrocarbons [6].

However, also another important concern, cracking reaction is usually occurred as the side reaction that resulting to decrease the selectivity of the desired product. Common ketonic decarboxylation operates at high temperatures (more than 300° C) and can produce significant amounts of by-products such as light fragments formed in several ways such as by cracking of the fatty acid chains or by decarboxylation of the fatty acid. The formation of these by-products restricts the overall selectivity and thus the yield of the desired ketone product. There has so far been a restricted understanding of the factors that affect relatively poor selectivity. In addition, the side reactions that cause the lower selectivity also tend to cause faster catalyst passivation [17, 19].

J. ABBOT (1989) was examined the possible involvement of both types of carbocation which types of acid site (Brønsted or Lewis) are active during the cracking reactions of alkanes under various conditions. Brønsted sites can produce initiation of cracking through protonation of the feed molecule to give a carbonium ion which can crack to produce a smaller alkane and an adsorbed carbenium ion, which can subsequently crack to yield an alkene and a smaller carbenium ion. Thus, cracking of linear alkanes on aluminosilicate catalysts can be accounted for by assuming reaction occurs only at Bronsted sites. [19].

Yury V. Kissin (2011) was explained about all cracking catalysts under mild condition performing relatively similarly in terms of the nature of cracked products (alkanes, alkenes, cycloalkanes, light aromatic compounds), although, of course, they differ in the overall activity, degree of coke formation, and so forth. Moreover, some

catalysts of a much lower activity, such as amorphous aluminosilicates and natural and modified clays, produce similar cracked products [20].

2.4 Catalysts and literature reviews

Amphoteric reducible metal oxides, mentioned as CeO_2, TiO_2, and ZrO_2, have been summarized to be the most active catalysts for ketonic decarboxylation. Consequently, acid-base properties or exposed surface cations/anions with coordination vacancies have been proposed to play a critical role in their superior ketonic decarboxylation activity [15]. Carboxylate species can be adsorbed over surface metal cations in a number of different forms during ketonic decarboxylation [6]. The carboxylates bind to Lewis acid sites of the surface either in monodentate or bidentate configurations these latter are generally more stable [21].

Moreover, the first investigated systematically activity of simple mono- and bimetallic oxides (Ag, Bi, Cd, Cu, In, Pb, Re, Cr, Mg, Zn, Ca, Ga, Sr, Ba, Al, Eu, Gd, V, Co, Fe, La, Mn, Zr, Ce, Th and U) deposited on the surface of inorganic supports in the ketonic decarboxylation of propanoic acid into 3-pentanone under the same conditions [22]. It was obviously shown that the studied oxides can be classified into three groups:

    i)   slightly active

    ii)   fairly active

    iii)   highly active

About the highly active group consists of catalysts containing oxides of Mn, Zr, Ce, Th, and U. No synergistic effect was noted between these oxides [6].

The adsorption and reactivity of carboxylic acids on zirconia have been done on the monoclinic phase, which is stable. Monoclinic zirconia (m-ZrO_2) has been identified as very suitable catalyst for this reaction [4], which has been identified as a material with excellent intrinsic catalytic activity, and selectivity for the ketonic decarboxylation with carboxylic acids as substrates.

The mechanism of ketonic decarboxylation of carboxylic acid involving two types of active sites-metal cations and oxygen groups is explained in Figure 6. Several proposals exist in the literature [6, 21] and include the following:
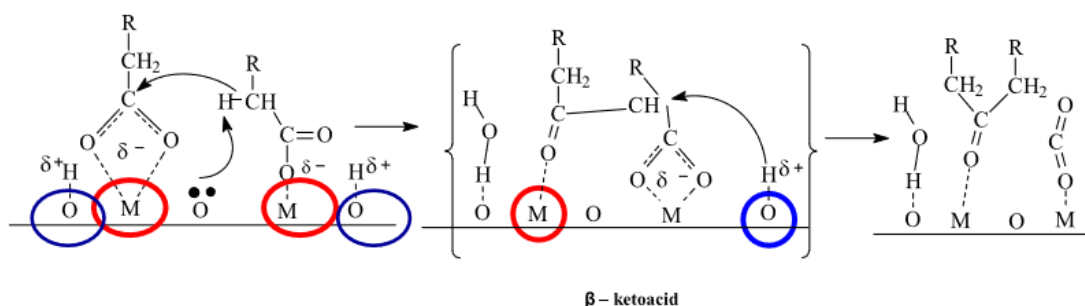
Figure 6 Mechanism of carboxylic acid ketonic decarboxylation

The changes in the catalyst surface cation composition affected the corresponding activity in ketonic decarboxylation. The origin of the changes is related to the reaction mechanism which involves metal cations catalytic sites (red circles) for carboxylate adsorption and stabilization along with oxygen-containing surface species (the lattice ions O^{2-} holding nucleophilic properties) in charge of absorption of the proton from –COOH group and α-hydrogen (blue circles). The resulting carboxylate ions through the participation of the surface hydroxyl groups, interact forming an intermediate compound, a β-ketoacid, which is then converted to a ketone upon decarboxylation.

A change in the binding type might play an important role in determining the ease with which the transition state is formed. There were various efforts reported in the literature aiming to resolve possible configurations of carboxylate adsorption species using different approaches. It is widely accepted that a neutral oxygen vacancy introduces two extra electrons in the lattice, which can be localized either in the created vacancy or in nearby cation sites. In ZrO_2 catalyst, the extra charge is trapped in the vacancy site rather than reducing the nearest Zr ions. Hence, there were three favored charge states for oxygen vacancies existed on surface of the ZrO_2: a neutral oxygen vacancy with the two electrons remaining at the oxygen vacancy, a singly charged oxygen vacancy, and a doubly charged oxygen vacancy [23].
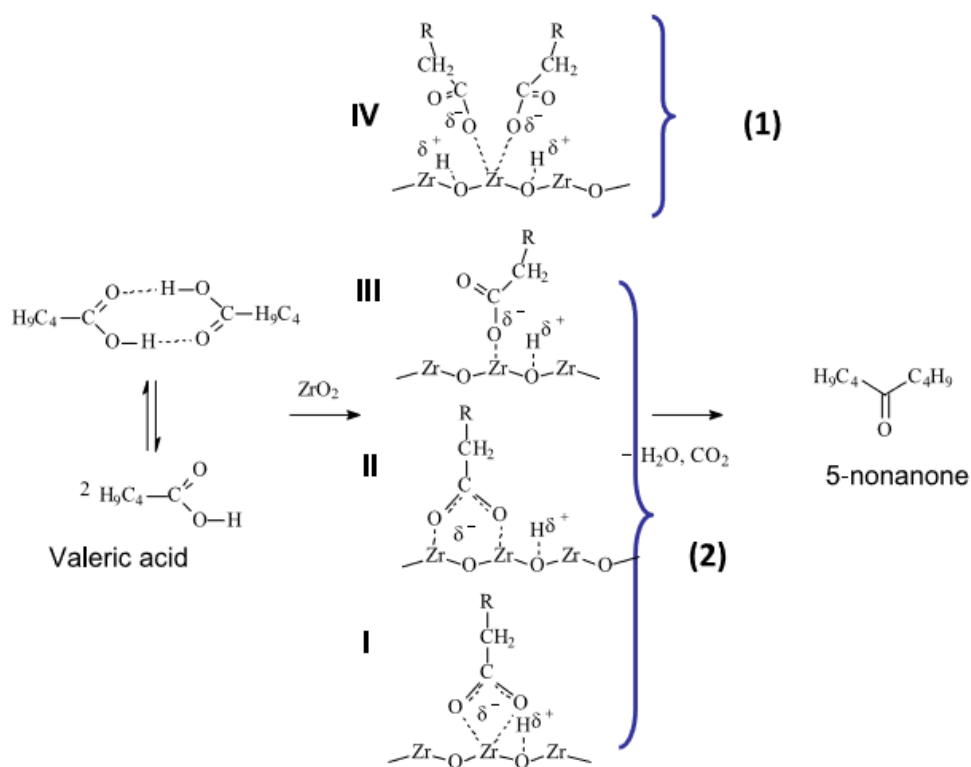
Figure 7 Mechanistic insight into ketonic decarboxylation of valeric acid with experimentally determined configurations of adsorbed valerates[6].

From Figure 7, this concept can be classified that all chemisorption forms of valeric acid on Lewis acid sites responsible for valeric acid transformation:

    i)   chelating bidentate valerates: (I)

    ii)   bridging bidentate valerates: (II)

    iii)   monomolecular monodentate valerates: (III)

    iv)   bimolecular monodentate valerates: (IV)

It can be divided two main pathways are involved that depending on the surface carboxylate intermediates:

Pathway 1: via interactions of two monodentates coordinated to the same Zr cation (IV).

Pathway 2: via interactions of the surface chelating bidentate (I) with either monomolecular bridging bidentate (II) or monomolecular monodentate valerate (III).

Based on surface studies, it has been concluded that the relative contribution of each route to the overall ketone formation over metal oxide surfaces depends on the reaction conditions.

However, it has been observed that doping zirconia with alkali metals or metal oxides result in an improved activity in the ketonic decarboxylation.

Glinski *et al.* (1995) demonstrated that ketonic decarboxylation can be catalyzed by many different oxides. To show this, they carried out the ketonic decarboxylation on 20 different metal oxides supported on silica. So, the amphoteric oxides (CeO_2, MnO_2, La_2O_3) appear to be better catalysts than pure acidic or basic oxides. At 400 ^{o}C, the 87-97% conversion were obtained [24].

A.G. Gasanov *et al.* (2013) was investigated that one of more faster using catalysts in reaction of decarboxylation are magnesium and titanium oxides. The optimal temperature of decarboxylation process on the MgO-catalyst is 350 ^{o}C. It provided the acid conversion maximum 94-96%, and the acid number decreasing to 1.5 mg KOH/g [25].

Yu. A. Zaytseva *et al.* (2013) was investigated ketonic decarboxylation of valeric acid, which can be obtained by lignocellulosic biomass conversion, was carried out in a fixed bed flow reactor over ZrO_2, 5–20 % CeO_2/ZrO_2 and CeO_2 both under hydrogen and nitrogen stream at 355 ^{o}C and atmospheric pressure. Regardless gas carrier 10 wt.% CeO_2/ZrO_2 was found to show higher catalytic activity compared to zirconia as well as other ceria modified zirconia while ceria exhibited very low catalytic activity [16], as shown in Table 4.

Table 4 Catalytic properties of CeO_2, ZrO_2 and 10 % CeO_2/ZrO_2 oxides in the ketonic decarboxylation of valeric acid in nitrogen gas[16].

Sample	Conversion (%)	Selectivity (%)	Surface area (m^2/g)
CeO_2	31	80	25
ZrO_2	66	80	105
10 % CeO_2/ZrO_2	82	81	79

Reaction conditions: 355 ^{o}C, 1 bar, N_2 flow rate 30 cm^3/min, LHSV of valeric acid 0.34 cm^3/(g h)

A. A. Shutilov *et al.* (2013) were examined about the phase composition, microstructure, and catalytic properties of the samples of ZrO_2 and CeO_2–ZrO_2 calcined in air at temperature 450–500℃ in the ketonic decarboxylation reaction of pentanoic acid were studied. It was discovered that ZrO_2 of tetragonal and monoclinic modifications is characterized by sufficiently high activity and selectivity for 5-nonanone; the yield of 5-nonanone was 66.3-64.9%. The modification of zirconia with cerium oxide leads to the formation of a substitutional solid solution based on tetragonal ZrO_2. Upon the addition of CeO_2 in an optimum amount of 10 wt.% to zirconia, an increase in the conversion of pentanoic acid was observed with the retention of high selectivity for the target product, which led to an increase in the yield of 5-nonanone to 73.3% [26].

It is well known that the synthesis of long-chain ketone products from long-chain esters is of great interest, but there are not enough of the investigations in this field.

Roman Klimkiewicz *et. al.* (2001) were studied ketonic decarboxylation of methyl esters of fatty acids over a catalyst that contained Sn, Ce, and Rh oxides in a molar ratio of 90:9:1. The applied raw material, diluted with methanol, was transformed at atmospheric pressure in the temperature range of 340–400℃. At the optimal temperature of 385℃ and 96% conversion of starting material, ketones were obtained with a total yield of 63% including 47% 18-pentatriacontanone, 3% 16-hentriacontanone, 6% methyl ketones, and 7% other ketones and the obtained product included 14% hydrocarbons (mainly saturated and unsaturated C_{18}) [18].

Borja Oliver-Tomas *et. al.* (2017) were studied the catalytic reaction carried out in a tubular fixed-bed continuous flow reactor. The reagent, methyl stearate, was heated to 50 ℃. The reactor was filled with 2.50 g of m-ZrO_2 diluted with silicon carbide. The reactions were carried out at temperatures between 400 and 550 ℃ at atmospheric pressure. Hydrogen gas was used as a carrier gas. The products were condensed at the exit of the reactor using an ice bath. At the lowest temperature, 400 ℃, the conversion of the methyl ester was 94%, being that completely converted at higher temperatures. The main product observed was the C35-ketone (approximately 30% yield. With increasing temperature, the yield of the C35-ketone gradually

decreased until it became zero at 450 °C. In this temperature range, C35-hydrocarbons (mainly alkenes) was observed as the main product, with the maximum yield (>40%) occurring at 450 °C. When the reaction temperature was increased above 500 °C, the yield of the C35-hydrocarbon fraction sharply decreased to almost zero [4].

A variety of acidic, basic, and amphoteric oxide catalysts have been investigated for ketonic decarboxylation of different carboxylic acids under various reaction conditions (375 °C and 400 °C). Glinski *et. al.* (1995) demonstrated that ketonic decarboxylation can be catalyzed by 20 different metal oxides supported on silica. The results are showed in Table 5.

Table 5 Activity of 10 wt % MOx/SiO$_2$ catalysts in ketonic decarboxylation of acetic acid[24].

Catalyst	Yield of acetone product	
	375 °C	400 °C
B$_2$O$_3$	2	3
MoO$_3$	4	5
WO$_3$	6	5
P$_2$O$_5$	10	12
V$_2$O$_5$	9	21
Bi$_2$O$_3$	11	18
NiO	31	-
Al$_2$O$_3$	15	37
CuO	29	39
ZnO	19	33
PbO	36	76
Cr$_2$O$_3$	48	39
Fe$_2$O$_3$	66	59
CoO	50	63
MgO	53	59
Nd$_2$O$_3$	22	61

La$_2$O$_3$	50	87
MnO$_2$	72	96
CdO	76	94
CeO$_2$	96	97

We also screen many catalysts for using in ketonic decarboxylation of methyl stearate. From Table 5, we can list the group of interesting catalysts and separate into two groups; (i) transition metal oxides group including CeO$_2$, Y$_2$O$_3$, and La$_2$O$_3$ and (ii) alkali metal oxides group including MgO and BaO with same 10% loading on ZrO$_2$ catalyst.

จุฬาลงกรณ์มหาวิทยาลัย

CHULALONGKORN UNIVERSITY

CHAPTER III

EXPERIMENTAL

This chapter provided the detail of chemicals, catalyst preparation, catalytic activity measurements, and catalyst characterization.

3.1 General

Methyl stearate (≥96%), Zirconium (IV) oxide powder (99%), Cerium (II) nitrate hexahydrate (99%), Yttrium (III) nitrate hexahydrate 99.9%, Lanthanum (III) nitrate hexahydrate 99.9%, and Barium chloride 99.9% were purchased from Sigma-Aldrich. Dodecane (>99%), and 18-pentatriacontanone (>95%) were purchased from TCI. Magnesium nitrate Hexahydrate (≥99%) was purchased from Fluka. And, Silicon carbide powder (coarse, 46 grit) was purchased from Alfa Aesar.

3.2 Catalyst Preparation

All of catalyst was prepared by incipient wetness impregnation method. The details of preparation method are present as follows:

3.2.1 Monoclinic zirconia (m-ZrO_2) support synthesis

Commercial monoclinic zirconia (m-ZrO_2) was used as support. The powder of the oxide was mixed with redistilled water until thin slurry and stirred for 2 h until homogeneous, then left to age for 16 h at room temperature. The resulted sol was dried in an oven at 110 °C for 24 h. The lumps were crushed and the sieved fractions of 0.40–0.80 mm were calcined at 600 °C for 3 h in air with the ramp rate 10 °C/min.

3.2.2 Modified metal oxide on monoclinic zirconia (m-ZrO_2) catalyst support

The catalysts were obtained by incipient wetness impregnation method with the following precursors: Cerium (III) nitrate hexahydrate ($Ce(NO_3)_3 \cdot 6H_2O$), Magnesium nitrate hexahydrate ($Mg(NO_3)_2 \cdot 6H_2O$), Yttrium (III) nitrate hexahydrate 99.9% ($YN_3O_9.6H_2O$), Lanthanum (III) nitrate hexahydrate 99.9% ($LaN_3O_9.6H_2O$), and Barium chloride 99.9% ($BaCl_2.2H_2O$). 3 g of m-ZrO_2 was doped with an aqueous solution of

each precursor to yield in 10 wt% of metal. The aqueous solution of metal precursor was slowly dropped onto m-ZrO$_2$ support to obtain the desired ratio. After impregnation, the pre-catalysts were dried in an oven at 110 °C for 24 h and calcined at 450 °C for 3 h in a stream of air with the ramp rate 10 °C/min. The catalytic systems containing 10 wt.% of active phase were noted as 10%CeO$_2$/ZrO$_2$, 10%Y$_2$O$_3$/ZrO$_2$, 10%La$_2$O$_3$/ZrO$_2$, 10%MgO/ZrO$_2$, and 10%BaO/ZrO$_2$, respectively.

3.3 Reactant

Using methyl stearate (≥96%) as substrate and dodecane (>99%) as diluent [27] and all reagents were used without any further purification. The liquid feed was contained 10%(w/v) methyl stearate in dodecane because this concentration had no waxing occurred. The suitable concentration, 10%(w/v), was obtained from our experimental with varying the concentration of substrate in the rage of 0-50%(w/v) and placed them in the ambient pressure and temperature for one month. We found that about 15-50%(w/v) has a solid wax occurred in the solution and 0-10%(w/v) has no wax occurred and still in liquid solution form. So, we conclude that the suitable concentration for diluting substrate is 10%(w/v).

3.4 Catalytic activity measurements

Gas phase ketonic decarboxylation reaction was carried out in a tubular fixed-bed continuous flow reactor (11.45 mm of internal diameter). The feed, in the case of 10%(w/v) methyl stearate in dodecane, was heated to 50 °C. The 2.50 g of catalyst diluted with silicon carbide was contained in the reactor. The reaction was performed at a temperature range of 400°C, 450°C, and 500°C at 1 bar, 10 bar, and 20 bar. Nitrogen gas (100 mL/ min) was employed as a carrier gas, and the reactant was fed using HPLC pump at 1.27 mL/min with a weight hourly space velocity (WHSV) of 3.06 h^{-1} (see in Appendix. A) during 30 min of time-on-stream. The products were condensed at the exit of the reactor using an ice bath. After finishing the reaction, we must clean up the line process by using dodecane solvent with same flow rate and 300 mL/min of nitrogen carrier gas for eliminating trace contaminants or remaining substrate in feed inlet that can cause wax blocking in the line process.

The liquid product was analyzed off-line by gas chromatography (GC) equipped with a flame ionization detector (FID) and a DB-1 capillary column (15m x 0.53mm x 0.15um). Then, the peak results were calculated with the calibration curve either liquid feed or ketone product for more accurate calculation.

According to the analysis of all products, the temperature program of GC-FID condition will be set up for the best detective performance as shown in Figure 8.
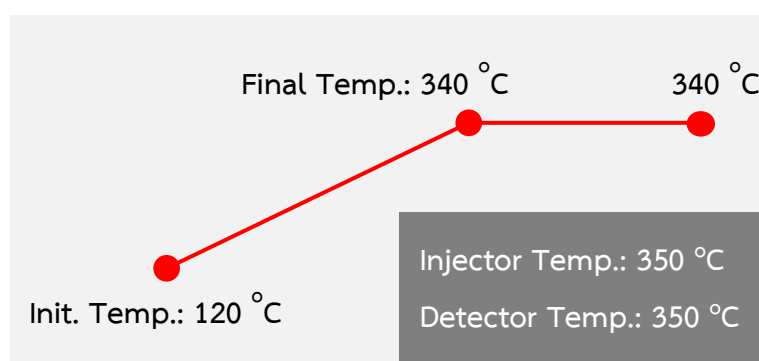
Figure 8 Temperature program of GC-FID condition.

The temperature of column was initially 120 $^{\circ}$C after injection, and therefore, the temperature was increased from 120 $^{\circ}$C to final temperature, 340 $^{\circ}$C with a ramp rate of 10 $^{\circ}$C/min then held for 10 min. The temperatures of injector and detector were 350 $^{\circ}$C because it must be higher than the column temperature for preventing liquid condensation before sample detected.

The conversion, selectivity, and cracking products were calculated from the following equations;

$$\text{Conversion (\%)} = \frac{\text{Moles of feed (in) - Moles of feed (out)}}{\text{Moles of feed (in)}} \times 100$$

$$\text{Selectivity (\%)} = \frac{\text{Moles of one product}}{\text{Moles of feed (in) - Moles of feed (out)}} \times 100$$

$$\text{Cracking (\%)} = \frac{\text{Amount of cracking by-products}}{\text{Amount of feed (in) - Amount of feed (out)}} \times 100$$

3.5 Catalyst characterization

The characterizations of catalyst were used by various techniques for understanding structure, properties and mechanism of catalyst. The details of each technique were described below:

3.5.1 X-ray diffraction (XRD)

The crystal structure and X-ray diffraction (XRD) patterns were analyzed by X-ray diffractometer (Bruker D8 Advance) using Cu-Kα irradiation at range between 10° and 80° with a step of 0.05 °s^{-1}. The lattice parameter and d-spacing were calculated based on Bragg's law.

3.5.2 Scanning electron microscope (SEM)

The elemental distribution on a surface of the catalysts was investigated with SEM-EDX using Link Isis series 300 program SEM (JEOL model JSM-5800LV).

3.5.3 N$_2$-physisorption

The surface area of catalysts was measured by the Brunauer–Emmet–Teller (BET) method on a Micromeritics ASAP 2020 instrument. The measurements were performed with nitrogen as adsorbate at liquid nitrogen temperature following the samples pretreatment at 300 °C under vacuum 8 h.

3.4.4 X-ray photoelectron spectroscopy (XPS)

XPS analysis using an ANICUS photoelectron spectrometer equipped with a Mg Kα that X-ray as a primary excitation and a KRATOS VISION2 software. XPS chart shown the binding energy (eV) of O1s region for catalysts was prepared by incipient wetness impregnation method. This O1s region signal consist oxygen vacancies respectively on the surface and subsurface regions for ZrO$_2$ and metal oxide modified ZrO$_2$ catalyst.

3.5.5 IR spectra of pyridine adsorption (Pyridine-IR)

The FT-IR of adsorbed pyridine was used to determine the Bronsted and Lewis acid sites of the sample with a Bruker Equinox 55 FT-IR spectrometer having a mercury cadmium telluride (MTCB) detector. The 0.05 g of catalyst sample was preheated at 500°C for 1 h with 10°C/min in a vacuum. After that the operating temperature was decreased to 40°C to absorb the pyridine for 30 min. The samples of catalyst were evacuated at 40°C for 1 h and the IR spectra was recorded at 40°C. The intensity of the Bronsted and Lewis acid sites in each sample was calculated from the subtraction of the IR spectra after sample pre-treatment from IR spectra of sample evacuation at 40°C for 1 h.

3.6 Design of reaction unit

This reaction unit was designed for ketonic decarboxylation reaction. There were many concerns about wax blocking in the line process. It was important to have no cold spots, especially at the reactor outlet and in case the formation of the heavy products was expected. The feed inlet without diluent and product outlet without heating line system can cause operability problems. In case the feed was a liquid and the reaction took place in the gas phase, the preheater temperature should be at least the boiling temperature of the feed in order to vaporize it. However, the temperature of the inlet lines would depend not only on the reaction temperature but also on the presence of components such as valves that may have temperature limits and the outlet lines had to be heated as well. Temperatures around 120-200°C were used, provided that all the components in the line would be stable at the chosen temperature. According to the heating line temperature should not exceed 160°C relating to the thermal resistant limitation of insulation. In this research, the usual temperatures for the feed inlet and product outlet line were 50°C and 120°C, respectively.

According to this reaction, the high temperature was used for operating, and the ramp rate was 10 °C/min, depending on the thermal stability of the catalyst. After the reaction, the reactor outlet was liquid mixture and containing a volatile fraction, then an ice bath should be used for collecting.

The P&ID diagram of the ketonic decarboxylation reaction line process, including feed section, reaction section and separating section, was designed and shown in Figure 9.

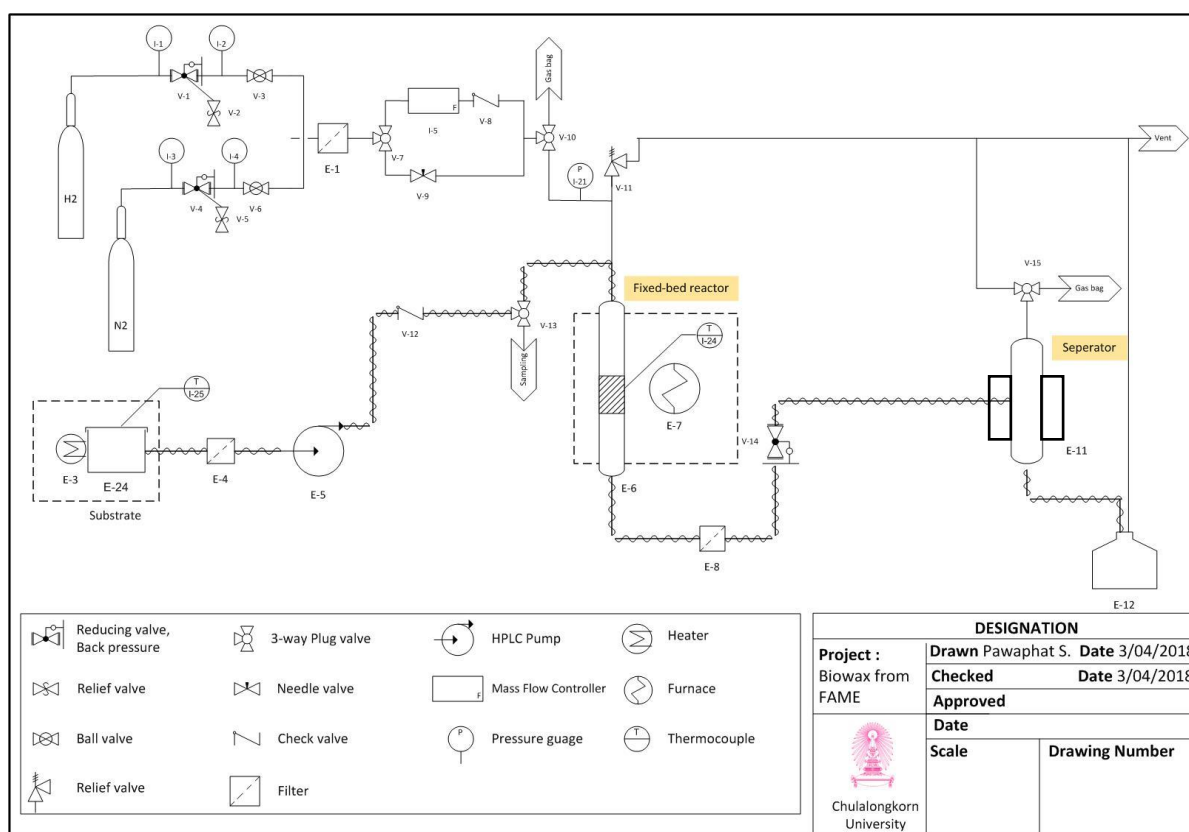Figure 9 P&ID diagram of the ketonic decarboxylation reaction line process, including feed section, reaction section and separating section.

The 3D model of structure and details of the ketonic decarboxylation reaction line process was designed and shown in Figure 10.
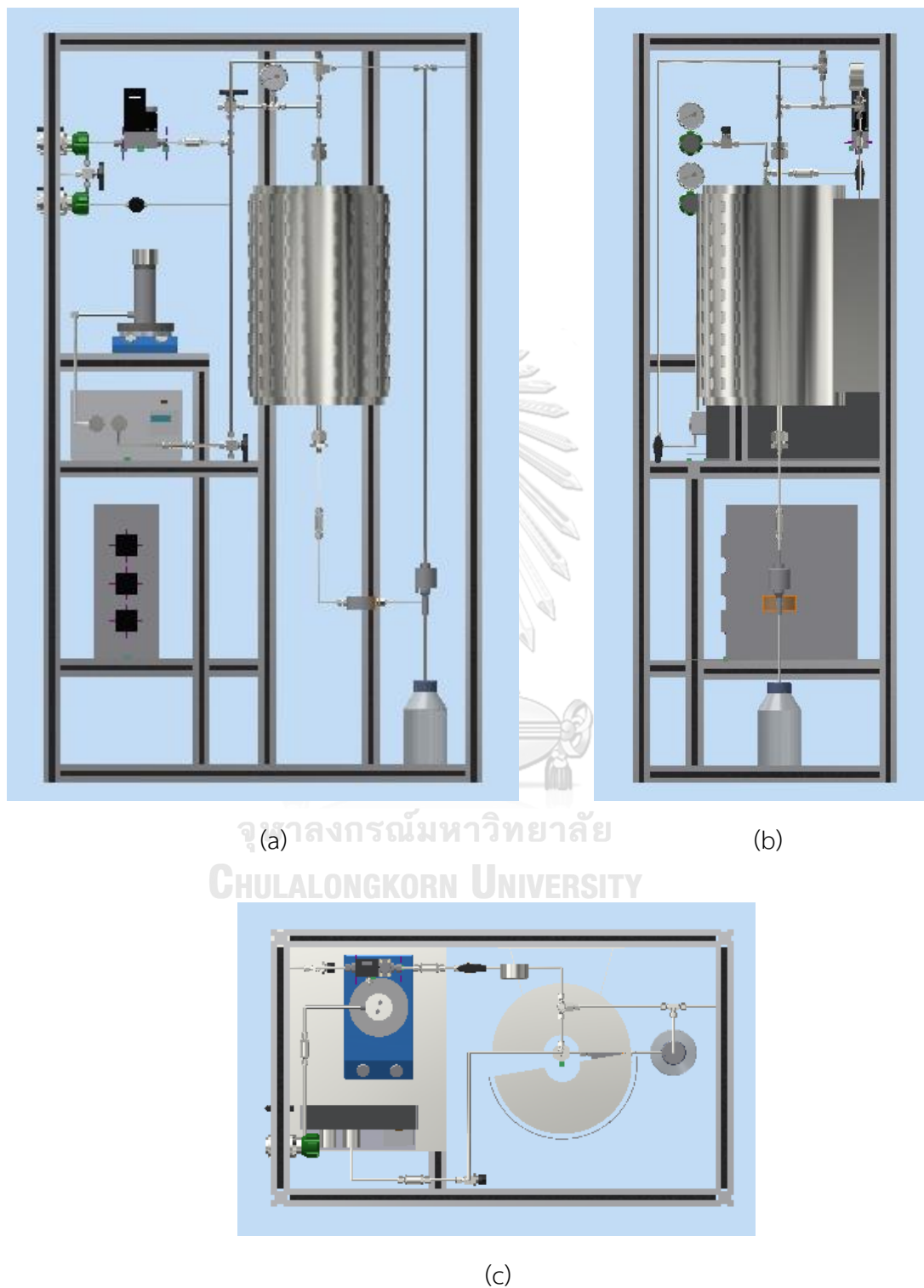

(a)

(b)

(c)

Figure 10 3D Model of the ketonic decarboxylation reaction line process

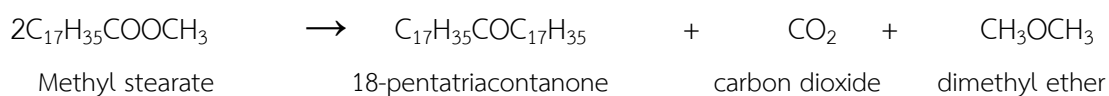(a) Front view (b) Side view and (c) Top view.

CHAPTER IV
RESULTS AND DISCUSSION

The results and discussion in this chapter are divided into four parts. In the first part, the effect of temperature and pressure on catalytic activity and selectivity was investigated for minimizing undesired cracking products. Furthermore, the optimal condition for operating in this reaction was founded and applied for testing with other metal oxide modified ZrO_2 catalysts. In the second part, the characteristics and catalytic properties of ZrO_2 and metal oxide modified ZrO_2 catalysts with the impregnation method have been evaluated in the gas phase via ketonic decarboxylation of methyl stearate at the optimal condition. Several techniques were used for characterization such as SEM, XRD, N_2-physisorption, XPS, and Pyridine-IR techniques. The specific characteristics of each catalyst has been demonstrated. Including to catalytic performances of all catalysts were compared in the gas phase ketonic decarboxylation and exhibited the conversion of methyl stearate and the selectivity of 18-pentatriacontanone ketone product in the third part. Moreover, the effect of oxygen vacancies and acidity of ZrO_2 and metal oxide modified ZrO_2 catalysts have been evaluated. And the last part, the key roles of catalytic properties about oxygen vacancy and two types of acid sites that effect on catalytic activity and selectivity of this reaction will be discussed. The results and discussion details of each part are described below:

4.1 Effect of temperature and pressure over ZrO_2 Catalyst

The ketonic decarboxylation of methyl stearate (C18:0) to 18-pentatriacontanone or stearone (C35) was carried out in gas-phase reaction at the varied high temperature with various pressures. The reaction was exhibited in the equation below:

$$2C_{17}H_{35}COOCH_3 \longrightarrow C_{17}H_{35}COC_{17}H_{35} + CO_2 + CH_3OCH_3$$

Methyl stearate   18-pentatriacontanone   carbon dioxide   dimethyl ether

The mainly C_{35} ketone product, 18-pentatriacontanone, is occurred after this reaction. And, carbon dioxide and dimethyl ether are produced as by-products in gas phase [6]. The effect of reaction temperature and pressure on the catalytic activity of ZrO_2 catalyst were determined by adjust the reaction temperature from 400-500 $^{\circ}$C and pressure varied from 1-20 bar. The conversion of methyl stearate in ketonic decarboxylation over ZrO_2 catalyst when adjusted the reaction temperatures and pressures is shown in Figure 11.
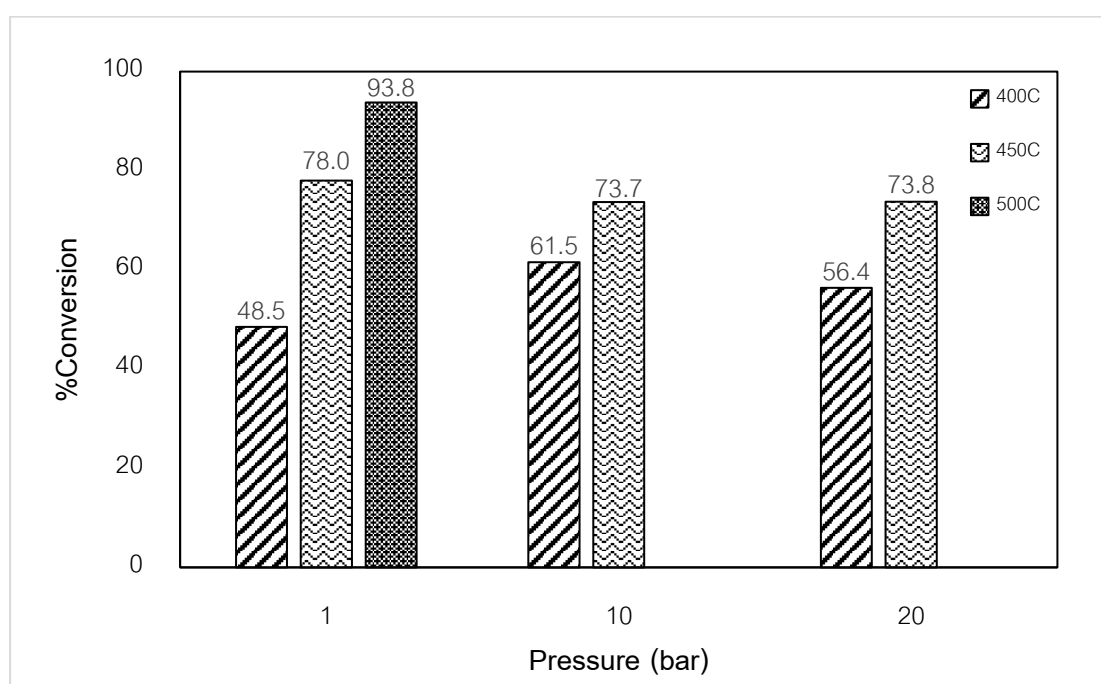
Figure 11 Conversion of methyl stearate in ketonic decarboxylation over ZrO_2 catalyst at different temperatures and pressures.

From Figure 11, at pressure 1 bar, the conversion of methyl stearate significantly increased from 48.5 to 93.8% when the reaction temperature enhanced from 400 to 500 $^{\circ}$C. In similarly, the conversion of methyl stearate increased from 61.5 to 73.7% and 56.4 to 73.8% when increased the reaction temperature from 400 to 450 $^{\circ}$C at pressure 10 and 20 bar, respectively. These can be suggested that higher temperatures strongly effect to increase ketonic decarboxylation activity and it was endothermic reaction. These results correspond with the concept of Le Chatelier's principle

equilibrium, an increase in temperature or pressure will affect the chemical equilibrium to forward the reaction [28]. However, the conversion of methyl stearate slightly decreased when increased the reaction pressure from 10 to 20 bar at the same temperature. This might be because methyl stearate was difficult to remove from the ZrO_2 surface or lower mass diffusion when using higher pressure. Therefore, the reaction activity was dropped when increased the reaction pressure.
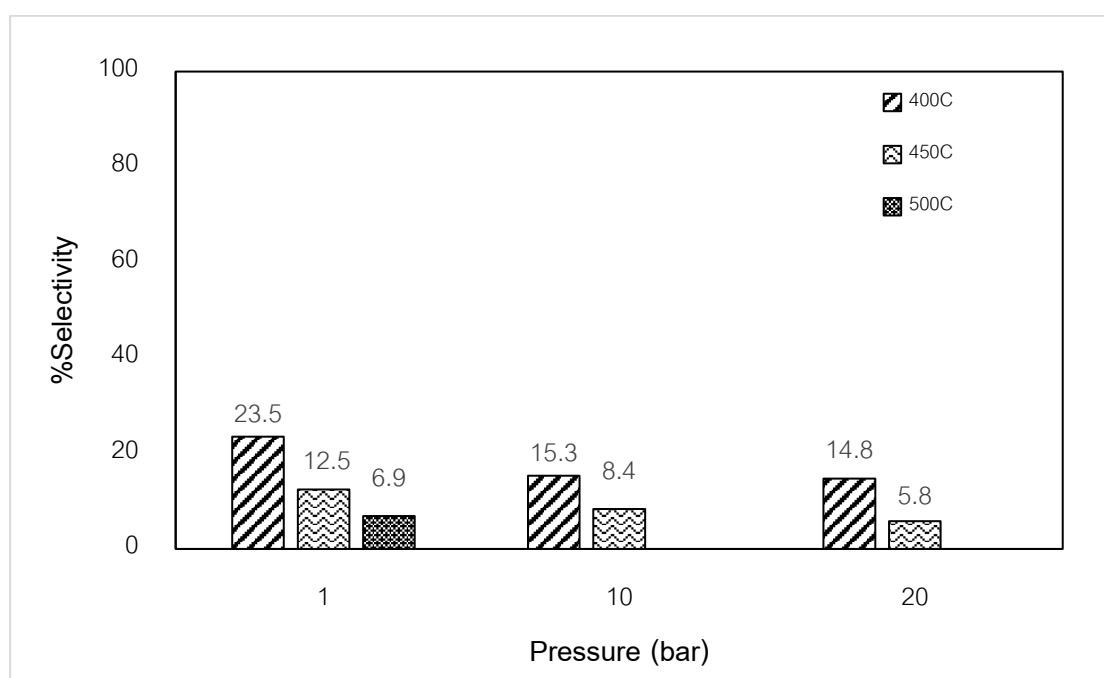
Figure 12 Selectivity of 18-pentatriacontanone (C35) in ketonic decarboxylation over ZrO_2 catalyst at different temperatures and pressures.

Considering the selectivity of 18-pentatriacontanone (C35), Figure 12 illustrates the selectivity for 18-pentatriacontanone over ZrO_2 catalyst with various reaction temperatures and pressures. According to the results, the selectivity of 18-pentatriacontanone at pressure 10 and 20 bar were found to be lower than the selectivity obtained at 1 bar. Moreover, enhancement of reaction temperatures from 400 to 500°C affect to reduce the selectivity of 18-pentatriacontanone since methyl stearate could be cracked to other products and the cracking products will be occurred

as a side reaction. However, the highest selectivity of 18-pentatriacontanone was 23.5% when the reaction temperature and pressure were 400 $^{\circ}$C and 1 bar.
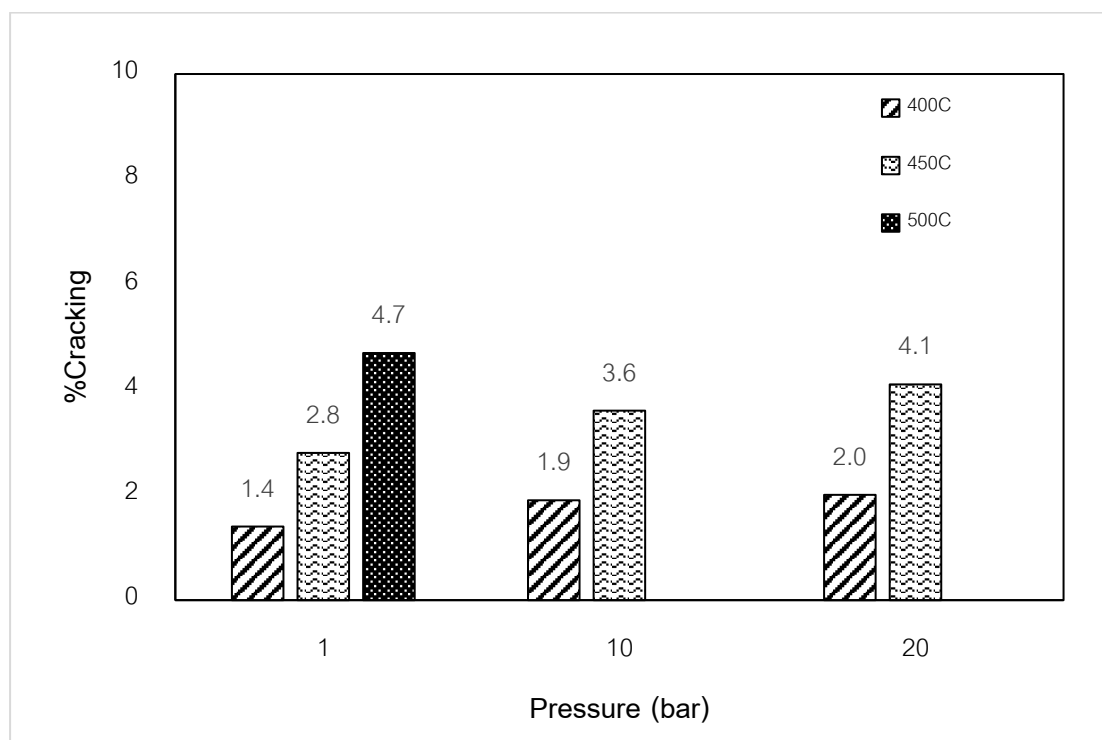
Figure 13 Catalytic cracking of by-products in ketonic decarboxylation over ZrO$_2$ catalyst at different temperatures and pressures.

The catalytic cracking of methyl stearate over ZrO$_2$ catalyst were investigated in terms of percent of cracking and the results are shown in Figure 13. The correlation between selectivity and cracking products can be confirmed the optimal condition which archived high activity and high selectivity. Higher cracking products indicated that reaction provides less amount of 18-pentatriacontanone or desired product than the cracking products. According to results, increasing of temperature was strongly influenced to increase cracking products whereas pressure did not have the significant effect. At 1 bar, when increased the reaction temperature from 400 to 450 $^{\circ}$C the cracking products increased from 1.4% to 2.8% and then continuously increase to 4.7% at 500 $^{\circ}$C. At 10 bar, when the temperature increased from 400 to 450 $^{\circ}$C, the cracking products were certainly increased from 1.9% to 3.6%. At 20 bar, when the temperature

was increased from 400 to 450 °C, the cracking products increased from 2.0% to 4.1%. However, the minimum cracking product can be obtained at 400 °C with 1 bar of pressure. Accordingly, from the experimental data. The optimum temperature and pressure, which gives the maximum cracking product reach to 1.4%, was found to be 400 °C at 1 bar.

These can be remarked that the optimum temperature and pressure for ketonic decarboxylation of methyl stearate using ZrO_2 catalyst that gives high catalytic activity with the maximum selectivity of 18-pentatriacontanone was 400°C at 1 bar with minimum cracking products formation. The increasing temperature plays a significant role in forming the cracking more than pressure. A loss of selectivity, especially occurring higher reaction temperature, is due to a side reaction of cracking.

4.2 Characterization of ZrO_2 and metal oxide modified ZrO_2 catalysts

In this part, the characteristics and catalytic properties of ZrO_2 and metal oxide modified ZrO_2 catalysts prepared by incipient wetness impregnation method were investigated in the ketonic decarboxylation reaction of methyl stearate as following:

4.2.1 SEM-EDX

The morphology, particles size and shape of ZrO_2 catalyst were revealed by SEM technique and the metals dispersion was exposed by EDX technique.

(a) ZrO_2

Figure 14 SEM-EDX image of ZrO_2 catalyst (a) SEM micrograph and (b) Zr dispersion from EDX technique.

According to the SEM-EDX image, Figure 14(a) exhibits the SEM image of ZrO_2. It can be observed that the most particles of ZrO_2 were in uniform spherical shape with an average particle size around 10-20 μm. And, Figure 14(b) shows Zr metals dispersion with well dispersed particles.

(b) 10%CeO_2/ZrO_2

Figure 15 SEM-EDX image of 10%CeO_2/ZrO_2 catalyst (a) SEM micrograph and (b) Ce dispersion from EDX technique.

According to the SEM-EDX image, Figure 15(a) shows the SEM image of 10%CeO_2/ZrO_2. It can be observed that the most particles of 10%CeO_2/ZrO_2 were in uniform spherical shape. And, Figure 15(b) shows Ce metals dispersion with well dispersed particles.

(c) 10%Y_2O_3/ZrO_2

Figure 16 SEM-EDX image of 10% Y_2O_3/ZrO_2 catalyst (a) SEM micrograph and (b) Y dispersion from EDX technique.

According to the SEM-EDX image, Figure 16(a) shows the SEM image of 10%Y_2O_3/ZrO_2. It can be observed that the most particles of 10%Y_2O_3/ZrO_2 were in uniform spherical shape. And, Figure 16(b) shows Y metals dispersion with well dispersed particles and spread massively.

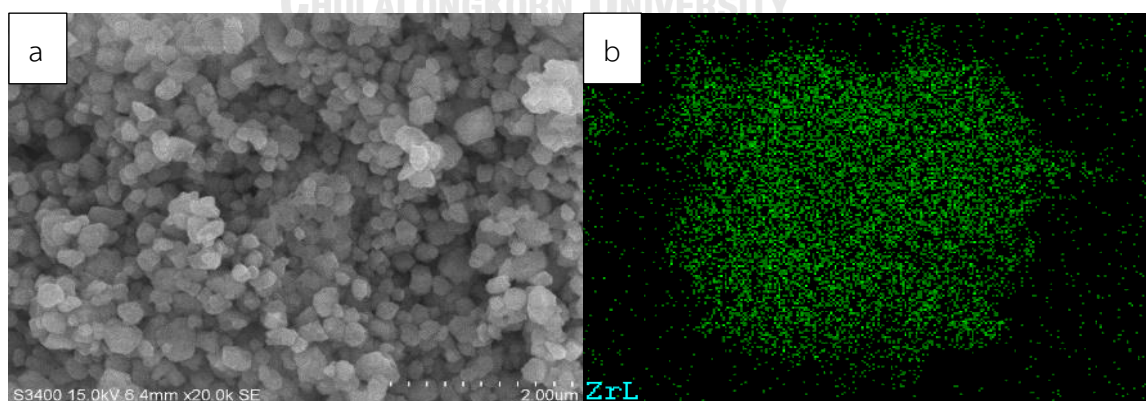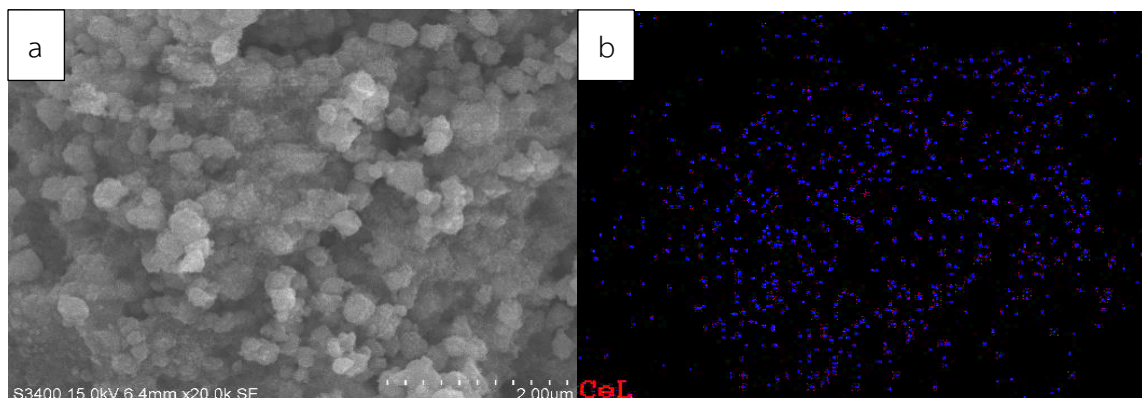(d) 10%La_2O_3/ZrO_2

Figure 17 SEM-EDX image of 10% La_2O_3/ZrO_2 catalyst (a) SEM micrograph and (b) La dispersion from EDX technique.

According to the SEM-EDX image, Figure 17(a) shows the SEM image of 10%La_2O_3/ZrO_2. It can be observed that the most particles of 10% La_2O_3/ZrO_2 were in uniform spherical shape. And, Figure 17(b) shows La metals dispersion with well dispersed particles.

(e) 10%$MgO3$/ZrO_2

Figure 18 SEM-EDX image of 10%MgO/ZrO_2 catalyst (a) SEM micrograph and (b) Mg dispersion from EDX technique.

From the SEM-EDX image, Figure 18(a) shows the SEM micrograph of the ZrO_2 assisted 10%MgO/ZrO_2 nanocomposite and the dispersed spherical morphologies were observed for the sample. And, Figure 18(b) shows Mg metals dispersion with well dispersed particles and spread massively.
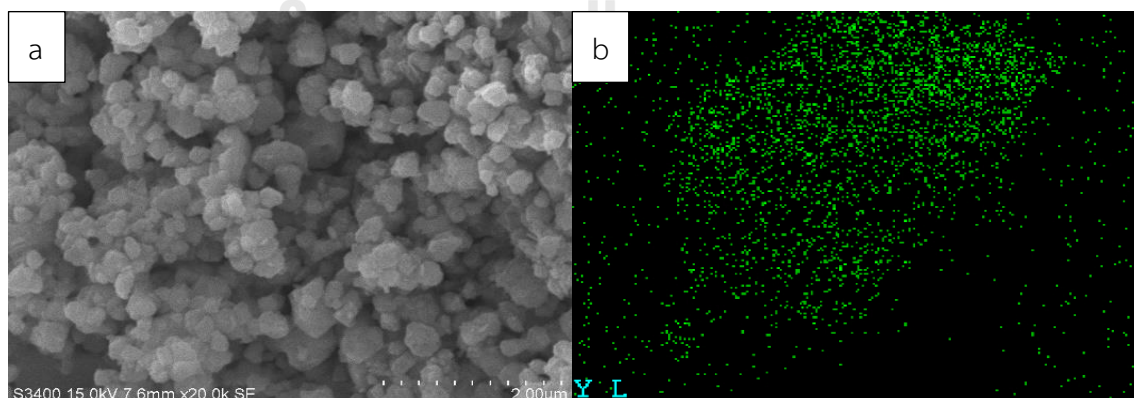
(f) 10%BaO/ZrO_2

Figure 19 SEM-EDX image of 10%BaO/ZrO_2 catalyst (a) SEM micrograph and (b) Ba dispersion from EDX technique.

From the SEM-EDX image, Figure 19(a) exhibits the SEM micrograph of the ZrO_2 assisted 10%BaO/ZrO_2 nanocomposite and the dispersed spherical morphologies were observed for the sample. And, Figure 19(b) shows Ba metals dispersion with well dispersed particles.
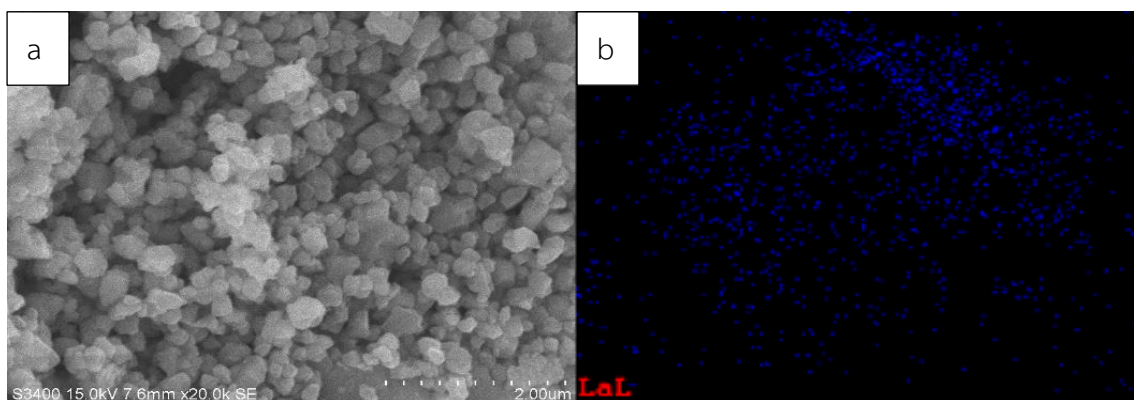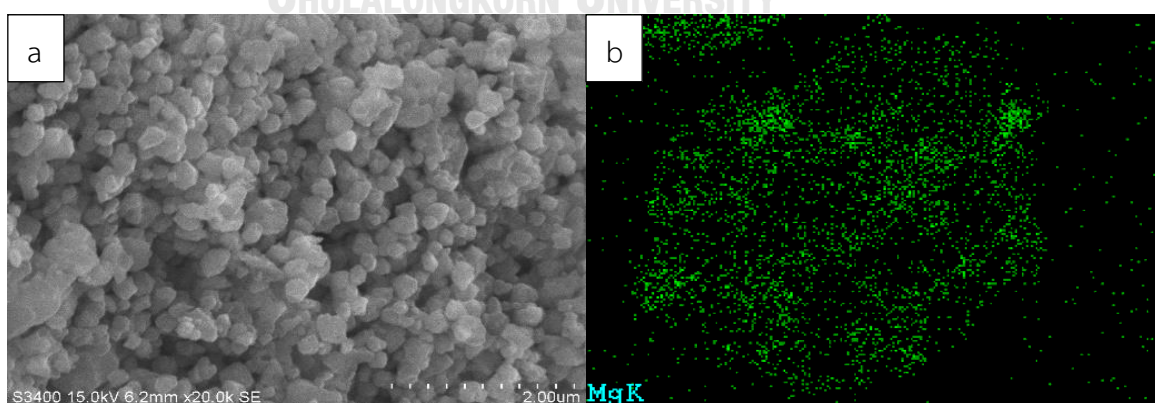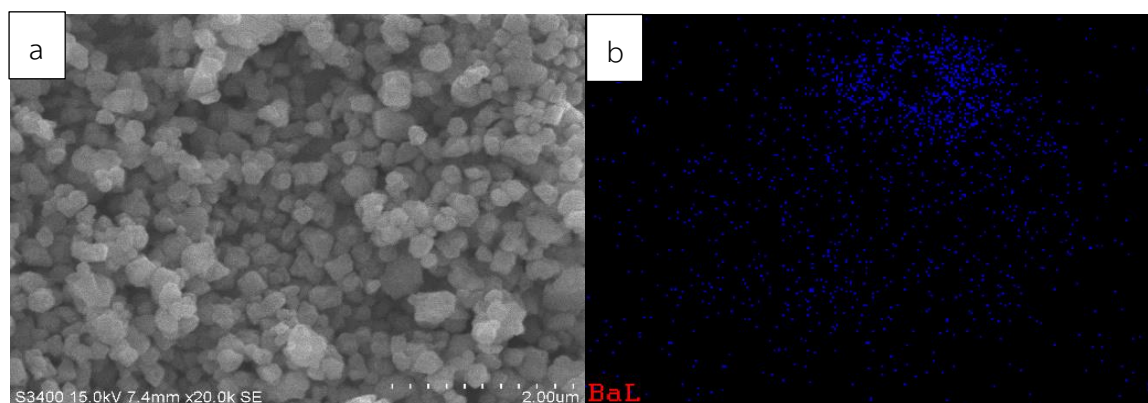
(g) 5%La_2O_3/ZrO_2
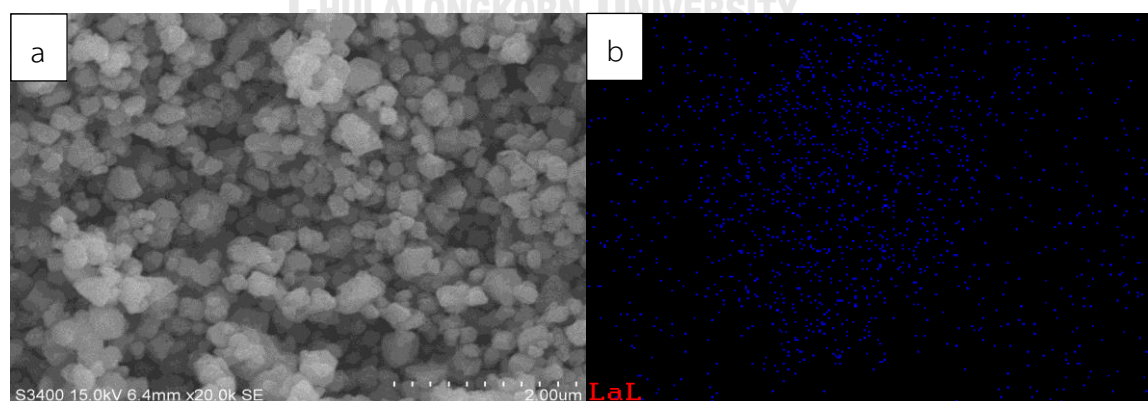
Figure 20 SEM-EDX image of 5% La_2O_3/ZrO_2 catalyst (a) SEM micrograph and (b) Ba dispersion from EDX technique.

From the SEM-EDX image, Figure 20(a) exhibits the SEM micrograph of the ZrO_2 assisted $5\%La_2O_3/ZrO_2$ nanocomposite and the dispersed spherical morphologies were mostly observed for this sample. And, Figure 20(b) shows La metals dispersion with well dispersed particles with lower than $10\%La_2O_3/ZrO_2$ catalyst.

Moreover, the atomic percentage of Zr and O in ZrO_2 supported catalyst were found to be 31.61 and 68.39, respectively. It was consisted well with 1:2 ratio of Zr/O which attributed to ZrO_2. In addition, the elemental analysis of ZrO_2 and metal oxide modified ZrO_2 catalysts, shown in Table 15 (Appendix B), exhibit the metal elements corresponding Zr, Ce, Y, La, Mg, and Ba that clearly observed in the atomic percentage of metal in ZrO_2 supported catalyst.

4.2.2 N_2-Physisorption

The surface area of catalysts is determined by physical adsorption of a gas on the surface of the solid called single-point BET (Nitrogen adsorption), the surface area of all catalysts is shown in Table 6.

Table 6 Nitrogen physisorption of ZrO_2 and metal oxide modified ZrO_2 catalysts

Sample	Surface area (m^2g^{-1})
ZrO_2	91.6
$10\%CeO_2/ZrO_2$	75.7
$10\%Y_2O_3/ZrO_2$	47.5
$10\%La_2O_3/ZrO_2$	40.4
$10\%MgO/ZrO_2$	42.2
$10\%BaO/ZrO_2$	33.2
$5\%La_2O_3/ZrO_2$	69.3

From Table 6, the pure ZrO_2 catalyst has the highest surface area around 91.6 m^2g^{-1}. Generally, materials for catalyst supports show high surface area, chemical stability as well as capability for dispersing metal particles highly over the surface [29].

After 10 wt.% of metal oxide (CeO_2, Y_2O_3, La_2O_3, MgO, and BaO) addition on ZrO_2 supported catalyst by the incipient wetness impregnation method, the data shows a decrease in surface area. When decreasing the metal oxide loading on catalyst, 5%La_2O_3/ZrO_2, the surface area will be increased when compared with 10%La_2O_3/ZrO_2 catalyst.

4.2.3 X-ray diffraction (XRD)

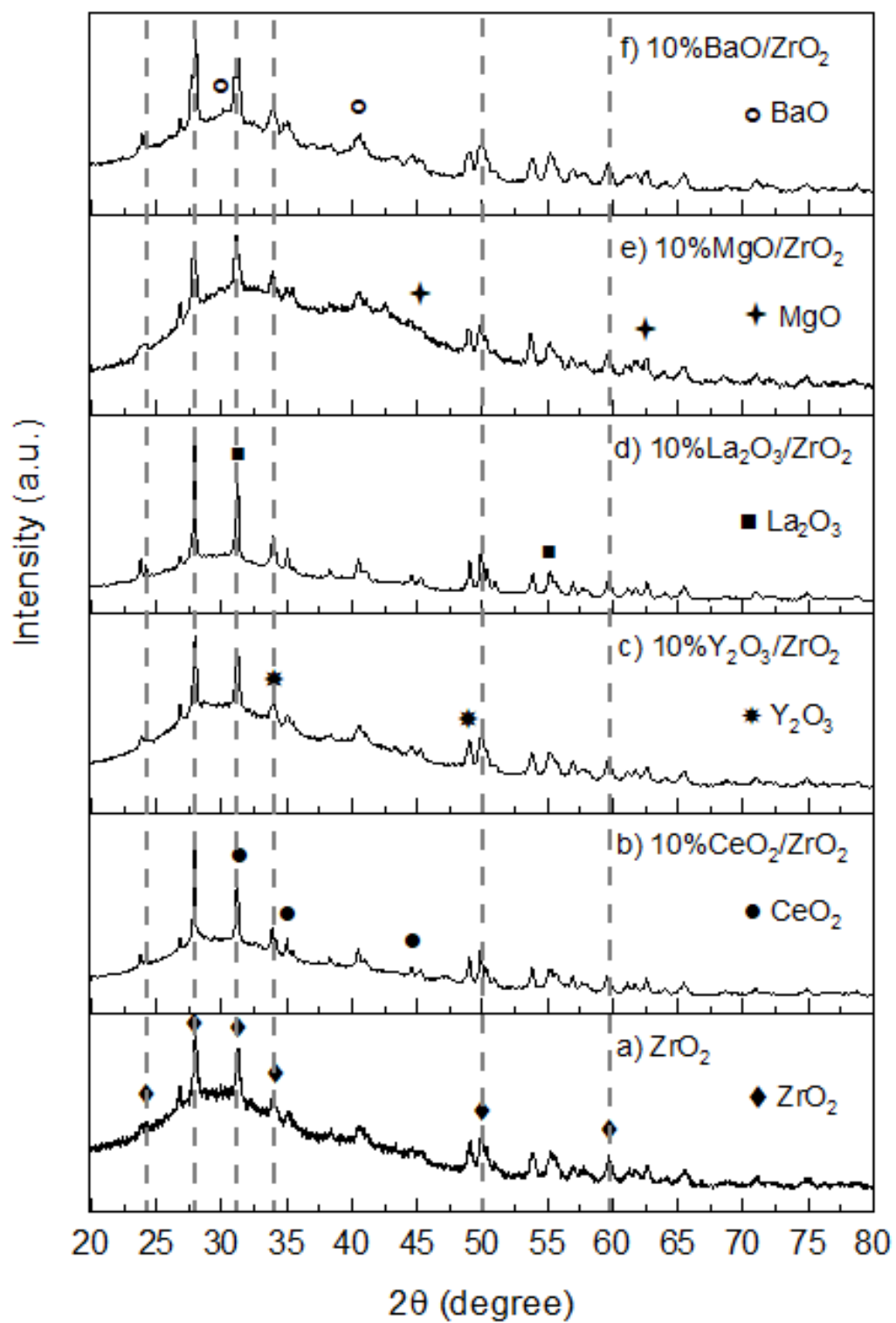The crystallite structure of the catalysts was confirmed by using X-ray diffraction techniques.

Figure 21 XRD patterns of ZrO_2 and metal oxide modified ZrO_2 catalysts.

The X-ray diffraction patterns of ZrO_2 supported catalyst and modified 10 wt% of metal oxide catalysts are displayed in Figure 21. The wide peaks varying between 25° and 45° can be attributed to ZrO_2 supported catalyst and modified 10 wt% of metal oxide catalysts in its amorphous state. For example, the XRD pattern of ZrO_2 assisted 10%CeO_2/ZrO_2 (b) nanocomposite, the four peaks in the pattern with 2θ values of 29.8, 34.4, 49.6 and 59.1 correspond to the (101), (002), (022) and (203) planes which indicates the formation of tetragonal and monoclinic structure of ZrO_2 [30]. Moreover, the XRD patterns of this catalyst exhibit the sharp peaks of the synthesized 10%CeO_2/ZrO_2 nanocomposites. No peaks were observed due to the impurities which confirm the formation of pure 10%CeO_2/ZrO_2 nanocomposite. Other catalysts likewise.

4.2.4 X-ray photoelectron spectroscopy (XPS)

X-ray photoelectron spectroscopy (XPS) technique is widely used in physical chemistry, which evaluated and analyzed characterization of the surface chemistry elemental composition, chemical state of the sample. Principle of this technique is considered by X-ray electron beam irradiation on the surface then photoelectron was released from the surface of sample. After that, the released photoelectron was analyzed and used to measure the kinetic energy of the released photoelectron in forms of binding energy and intensity of photoelectron peaks, which presented by trace amount of carbon and high solution of O1s state [31]. The binding energy (eV) of Oxygen Vacancy (O1s) state of catalysts are shown in Table 7 and Figure 22.

Table 7 Binding energy of O1s XPS spectra of ZrO_2 and metal oxide modified ZrO_2 catalysts.

Sample	Binding Energy (eV)
	Oxygen Vacancy (O 1s)
ZrO_2	2665.07
10%CeO_2/ZrO_2	9515.56
10%Y_2O_3/ZrO_2	4620.12
10%La_2O_3/ZrO_2	2556.76
10%MgO/ZrO_2	2384.06
10%BaO/ZrO_2	2082.26
5%La_2O_3/ZrO_2	1733.03
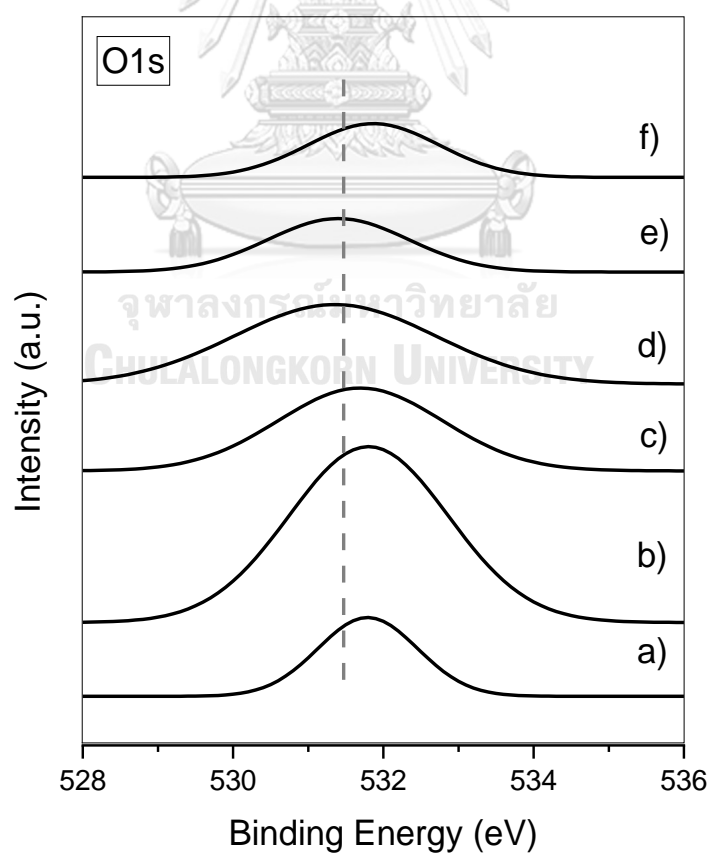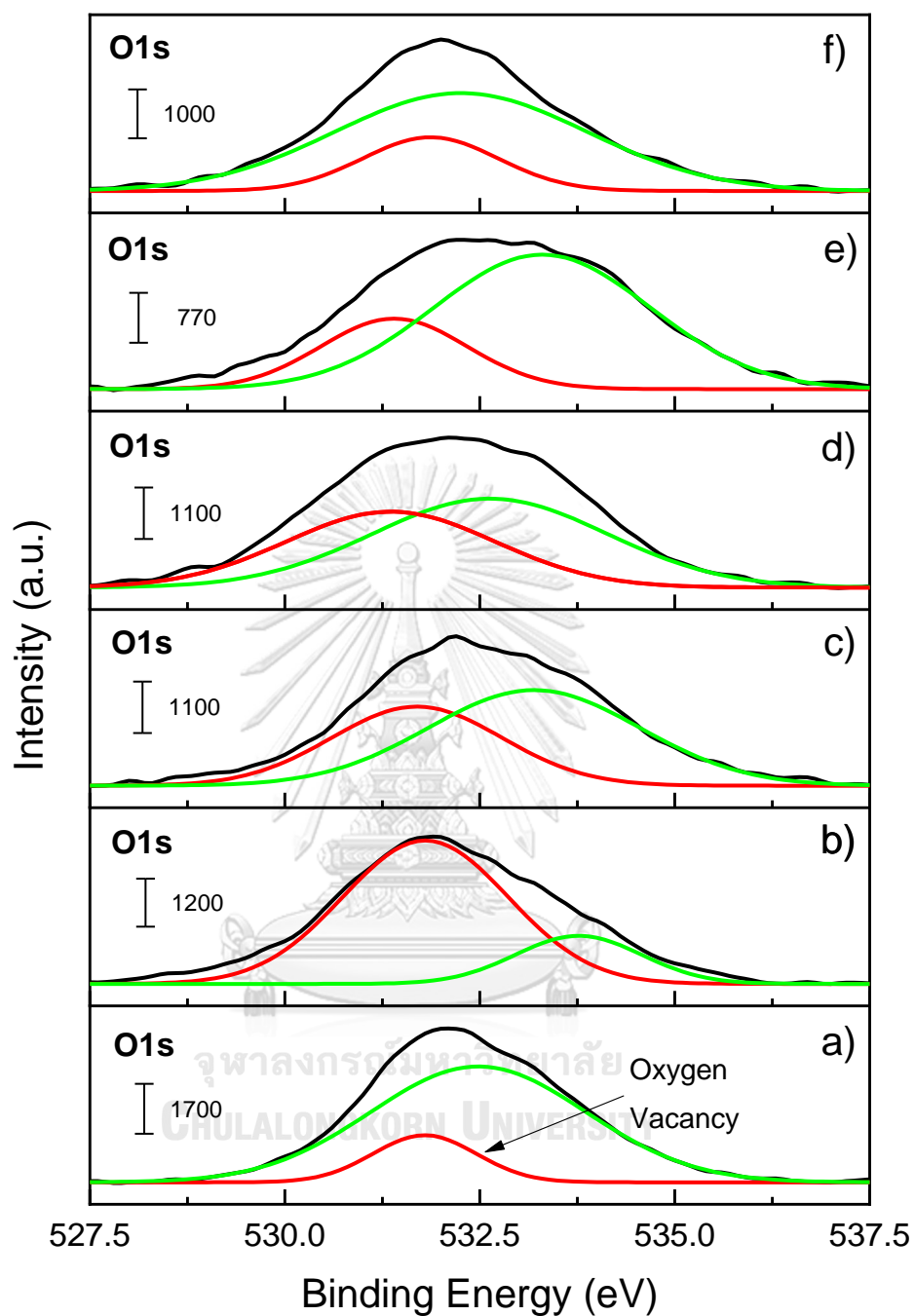
Figure 22 O1s XPS spectra of ZrO_2 and modified metal oxide on catalysts, which were deconvoluted by Gaussian fitting curve, including ZrO_2 (a), 10%CeO_2/ZrO_2 (b), 10%Y_2O_3/ZrO_2 (c), 10%La_2O_3/ZrO_2 (d), 10%MgO/ZrO_2 (e), and 10%BaO/ZrO_2 (f).

On deconvolution of the XPS spectra, it resolved into two distinguishable peaks centered at 530.5 and 531.9 eV corresponding to the lattice oxygen and non-lattice oxygen (i.e. oxygen vacancy), respectively [32]. A prominent surface alteration in the form of defects or disorders associated with the oxygen vacancy in ZrO_2 and modified metal oxide on catalysts was quite affected the selectivity of desired ketone product. The above results confirm that the disordered states of $10\%CeO_2/ZrO_2$ catalyst present higher amount of O1s binding energy than other catalysts, which creates large amount surface defects via oxygen vacancies. From Figure 20, red lines were represented to as well.

4.2.5 IR spectra of pyridine adsorption (Pyridine-IR)

The quantitative calculation of Lewis and Brønsted acid sites was determined by the integrated area of the adsorption bands at about 1540 and 1450 cm−1, respectively [33]. The acidity of Lewis and Brønsted acid sites was calculated by using the adsorption of Pyridine and reported in term of pyridine-IR spectra. Moreover, the concentration of Lewis and Brønsted acid sites of ZrO_2 and metal oxide modified ZrO_2 catalysts are calculated from the integrated area of typical bands are presented in Table 8.

Table 8 Surface acidity of ZrO_2 and metal oxide modified ZrO_2 catalysts.

Sample	Wavenumbers (cm^{-1})	Area of pyridine adsorption	Total Lewis acid (a.u./g)	Total Brønsted acid (a.u./g)
ZrO_2	1442.54	1.7020	52.53	5.10
	1539.88	0.1652		
$10\%CeO_2/ZrO_2$	1440.22	2.7050	86.70	2.10
	1540.51	0.0655		
$10\%Y_2O_3/ZrO_2$	1441.13	2.2386	67.02	4.80
	1540.52	0.1603		
$10\%La_2O_3/ZrO_2$	1440.05	3.0750	65.01	7.00
	1541.19	0.3311		
$10\%MgO/ZrO_2$	1440.70	1.0487	33.29	8.50
	1539.90	0.2678		
$10\%BaO/ZrO_2$	1440.66	0.6065	17.73	23.90
	1539.33	0.8174		
$5\%La_2O_3/ZrO_2$	1440.68	0.9324	28.6	3.8
	1541.17	0.1239		

The results from Table 8 show that all catalysts also have the large amount of total Lewis acid site more than the amount of total Brønsted acid site, except that on $10\%BaO/ZrO_2$ catalyst. The loading of transition metal oxides (Ce, Y, and La) on ZrO_2 supported catalyst resulted in a noticeable increase in the amount of total Lewis acid site. The $10\%Y_2O_3/ZrO_2$ and $10\%La_2O_3/ZrO_2$ were founded to have similar the Lewis acid site. On the other hand, the amount of Brønsted acid site of transition metal oxide (Ce, Y, and La) loading were investigated that lower than the loading of alkali metal oxides (Mg and Ba) on ZrO_2 supported catalyst. In this group, the $10\%MgO/ZrO_2$ and $10\%BaO/ZrO_2$ were founded to have similar the Brønsted acid site. About the

decreasing metal loading, 5%La$_2$O$_3$/ZrO$_2$, shows the lower Lewis acid site and Brønsted acid site than 10%La$_2$O$_3$/ZrO$_2$ catalyst.
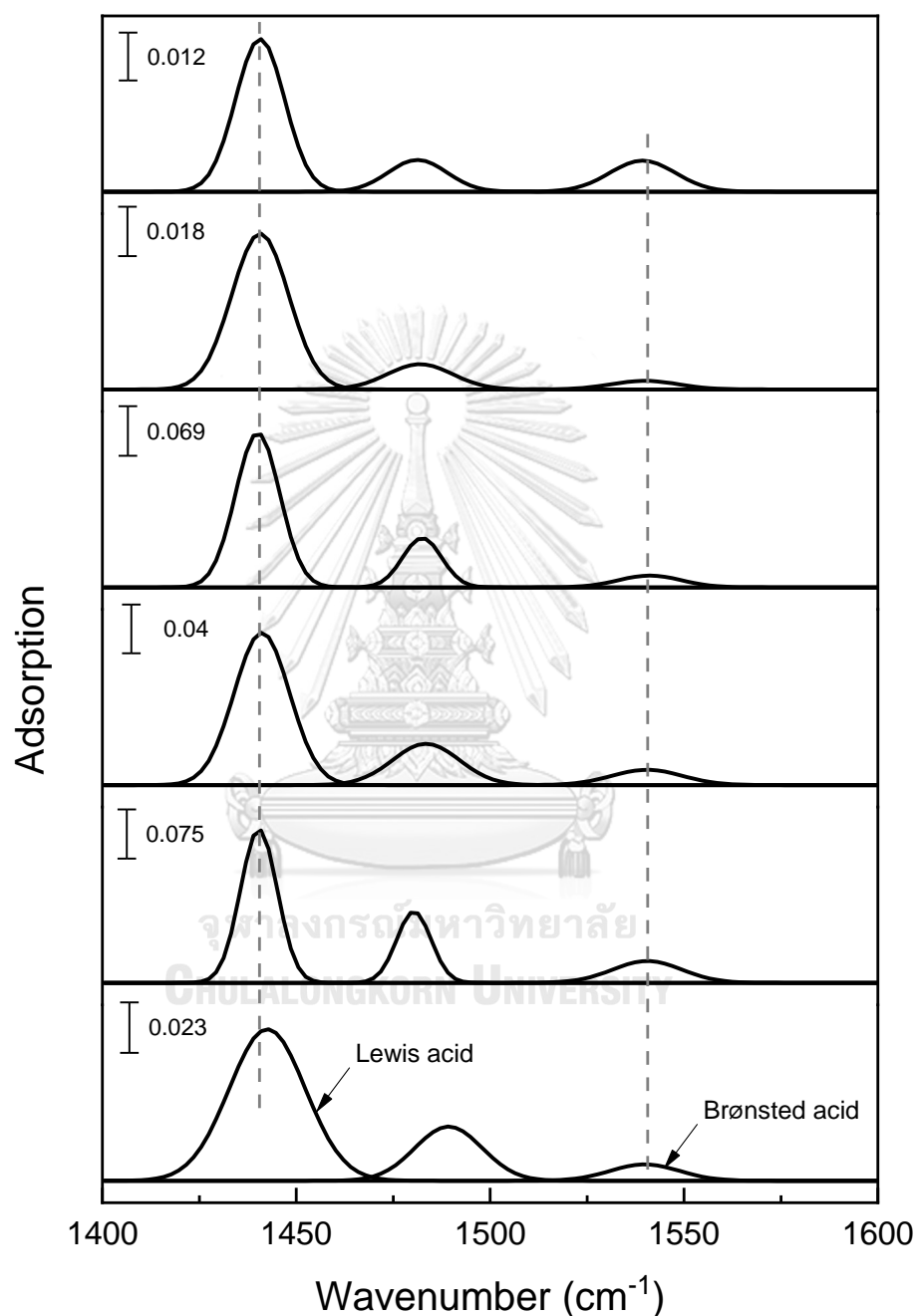
Figure 23 In situ FTIR transmission spectra of chemisorbed pyridine on ZrO$_2$ and metal oxide modified ZrO$_2$ catalysts., including ZrO$_2$ (a), 10%CeO$_2$/ZrO$_2$ (b), 10%Y$_2$O$_3$/ZrO$_2$ (c), 10%La$_2$O$_3$/ZrO$_2$ (d), 10%MgO/ZrO$_2$ (e), and 10%BaO/ZrO$_2$ (f).

In situ FTIR of Pyridine adsorbed samples was undertaken to probe their acid properties from Figure 23: Pyridine bound to Lewis acid sites gives characteristic vibrational bands at 1445–1440 cm^{-1}, whereas Pyridine bound to Brønsted acid sites gives characteristic vibrational bands at 1545–1535 cm^{-1}.

4.3 Effect of metal oxide modified ZrO_2 catalysts at the optimal condition via ketonic decarboxylation.

4.3.1 The conversion of methyl stearate and selectivity to 18-pentatriacontanone on metal oxide modified ZrO_2 catalysts.

The important question to be considered is related to the role of metal oxide modified ZrO_2 catalysts in ketonic decarboxylation. From Chapter 4.1, the optimal condition from testing with ZrO_2 catalyst that performing a high conversion, high selectivity with minimum cracking products occurred. The Figure 24 illustrates the conversion of methyl stearate in ketonic decarboxylation over metal oxide modified ZrO_2 catalysts at the optimal condition, $400^{o}C$, and 1 bar. The highest conversion of methyl stearate can be achieved from $10\%CeO_2/ZrO_2$ around 58.5%. The conversion slightly decreased to 50.3% for $10\%Y_2O_3/ZrO_2$ catalyst, and 50.1% for $10\%La_2O_3/ZrO_2$ catalyst. These two catalysts were able to be converted esters likewise. Followed by $10\%MgO/ZrO_2$ (47.2%), $10\%BaO/ZrO_2$ (44.1%), and $5\%Y_2O_3/ZrO_2$ (32.2%), respectively. The transition metal oxides ($10\%CeO_2/ZrO_2$, $10\%Y_2O_3/ZrO_2$, and $10\%La_2O_3/ZrO_2$) group also has higher catalytic activity than the alkali metal oxides group ($10\%MgO/ZrO_2$ and $10\%BaO/ZrO_2$) with same loading (10%).
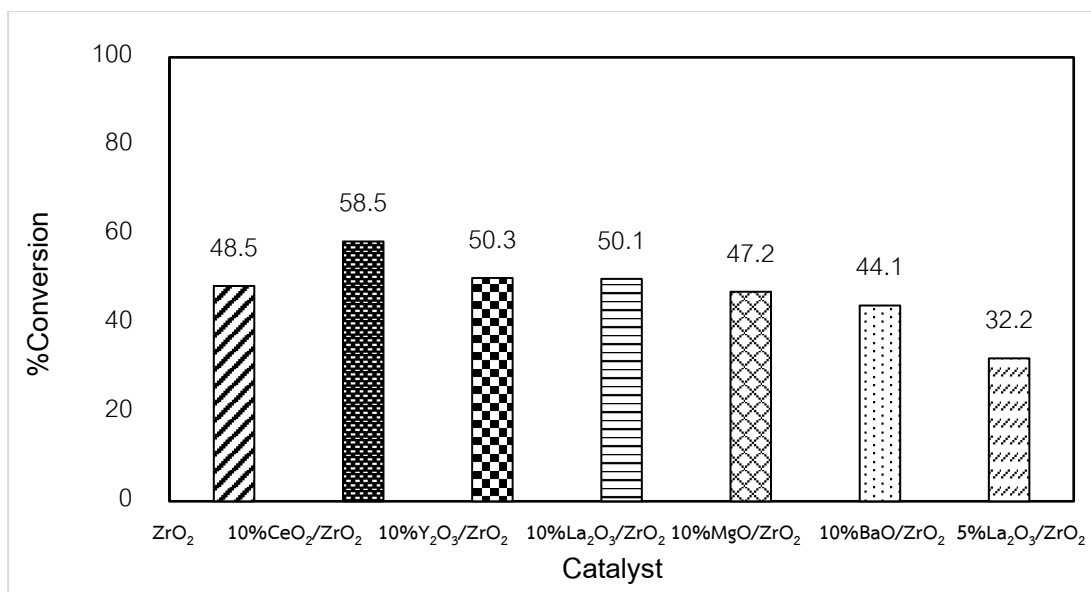
Figure 24 Conversion of methyl stearate in ketonic decarboxylation over metal oxide modified ZrO_2 catalysts at the optimal condition, 400°C and 1 bar.

At this optimum condition (400°C and 1 bar), Figure 25 shows that the selectivity goes through the maximum achieved 38.7% at $10\%CeO_2/ZrO_2$ catalyst. Surprisingly addition of a only small amount of relatively inactive ceria resulted in a noticeable increase of ZrO_2 activity [6]. Followed by 28.4%of selectivity from $10\%Y_2O_3/ZrO_2$ catalyst like conversion. ZrO_2 and $10\%La_2O_3/ZrO_2$ catalyst was found to demonstrate very similar value of selectivity, 23.5% and 22.0%. There is significant for the catalytic properties of these two catalysts. If the loading of metal oxide on catalyst decreased, the selectivity will be deceased too, for example, $5\%La_2O_3/ZrO_2$ catalyst providing 14.2%. The alkali metal oxides group ($10\%MgO/ZrO_2$ and $10\%BaO/ZrO_2$) perform lower selectivity to desired ketone product at 10.7% and 6.6%, respectively.
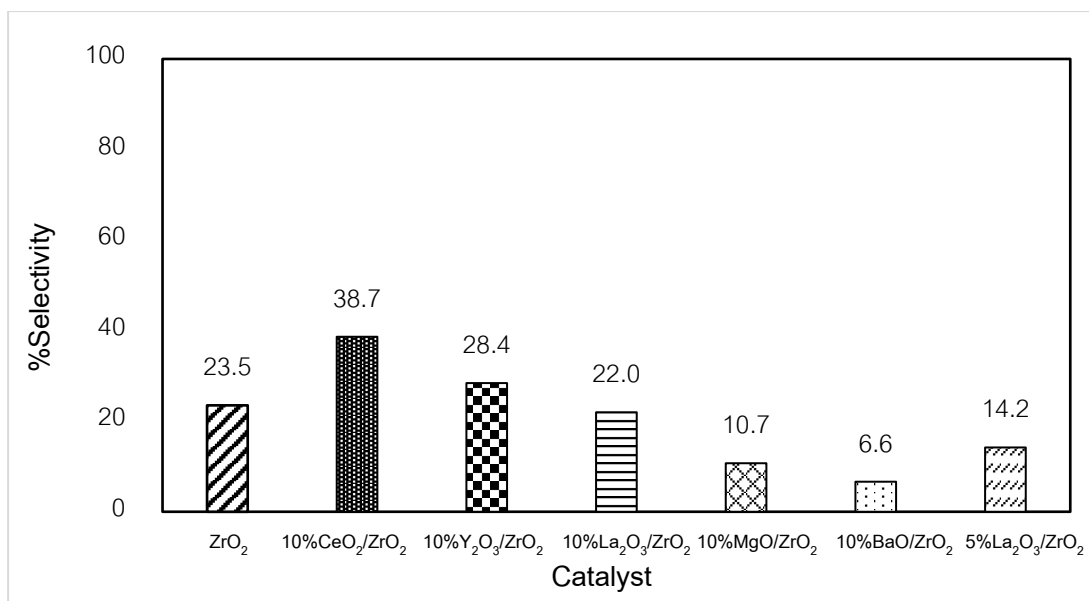
Figure 25 Selectivity of 18-pentatriacontanone in ketonic decarboxylation over metal oxide modified ZrO_2 catalysts at the optimal condition, 400°C and 1 bar.

4.3.2 The amount of cracking products formation on metal oxide modified ZrO_2 catalysts.

Although the minimum of cracking products occurred under this optimal condition when using pure ZrO_2 catalyst, the cracking products can be occurred as side reaction by using metal oxide modified catalysts in different values. Figure 26 shows cracking products of the transition and alkali metal oxide group modified ZrO_2 catalyst. The alkali metal oxides group (10%MgO/ZrO_2 and 10%BaO/ZrO_2) modified ZrO_2 catalyst produced the high content of cracking products approx. 1.9-2.4%. It will be considered likely a bad trend. So, we considered about the transition metal oxides (10%CeO$_2$/ZrO_2, 10%Y$_2$O$_3$/ZrO_2, and 10%La$_2$O$_3$/ZrO_2) group modified ZrO_2 catalyst also has a low content of cracking products around 0.7%, 1.2%, and 1.5%, respectively. Thus, the 10%CeO$_2$/ZrO_2 catalyst becomes more interested than another catalyst, because it has the lowest cracking products for this reaction condition.
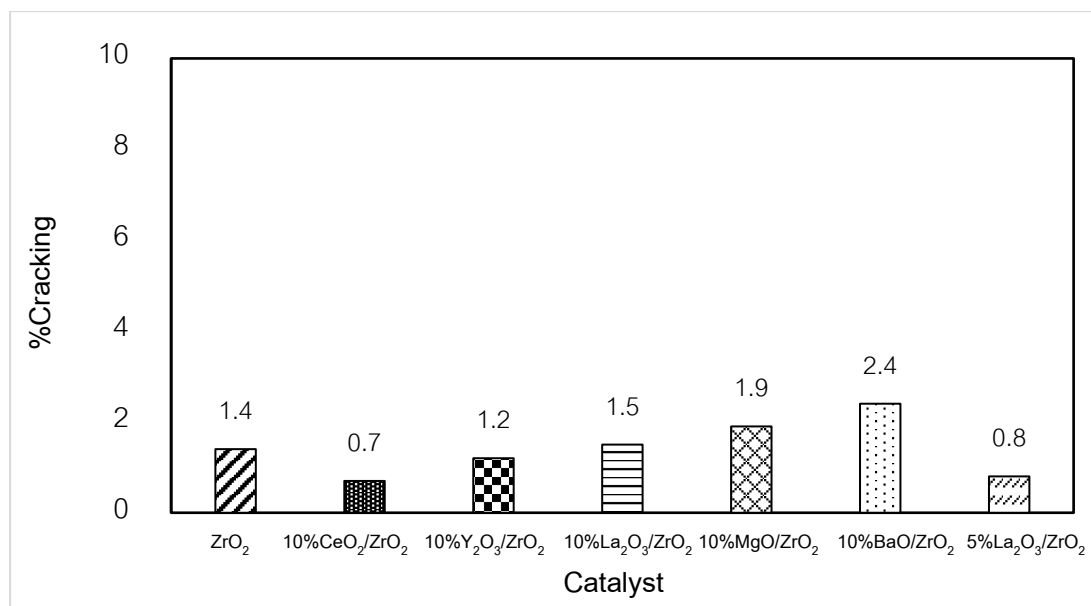
Figure 26 Cracking products in ketonic decarboxylation over metal oxide modified ZrO_2 catalysts at the optimal condition, $400^\circ C$ and 1 bar.

4.4 Comparative study the characteristics and catalytic properties of ZrO_2 and metal oxide modified ZrO_2 catalysts affect the catalytic performance.

In this part, the characteristics of catalysts including ZrO_2, $10\%CeO_2/ZrO_2$, $10\%Y_2O_3/ZrO_2$, $10\%La_2O_3/ZrO_2$, $10\%MgO/ZrO_2$, and $10\%BaO/ZrO_2$ were investigated by means of X-ray photoelectron spectroscopy (XPS) technique and IR spectra of pyridine adsorption (Pyridine-IR) to evaluate the binding energy of oxygen vacancies and amount of two types of acid sites, respectively.

Table 9 Catalytic performance and catalytic properties in ketonic decarboxylation of methyl stearate to 18-pentatriacontanone by using ZrO_2 and metal oxide modified ZrO_2 catalysts.

Caatalysts	Conversion[a] (%)	Selectivity[b] (%)	Cracking[c] (%)	Binding Energy O1s [d] (eV)	Total Lewis acid site[e] (a.u./g)	Total Brønsted acid site[e] (a.u./g)
ZrO_2	48.5	23.5	1.4	2665.07	52.53	5.1
$10\%CeO_2/ZrO_2$	58.5	38.7	0.7	9515.56	86.70	2.1
$10\%Y_2O_3/ZrO_2$	50.3	28.4	1.2	4620.12	67.02	4.8
$10\%La_2O_3/ZrO_2$	50.1	22.0	1.5	2556.76	65.01	7.0
$10\%MgO/ZrO_2$	47.2	10.7	1.9	2384.06	33.29	8.5
$10\%BaO/ZrO_2$	44.1	6.6	2.4	2082.26	17.73	23.9
$5\%La_2O_3/ZrO_2$	32.2	14.2	0.8	1733.03	28.6	3.8

[a] Reaction condition: Temperature = 400°C, Pressure = 1 bar, WHSV^{-1}= 3.02 h^{-1}, 2.5 g of catalyst, N_2 carrier gas

[b] Selectivity of 18-pentatriacontanone (C_{35}) ketone product

[c] Other by-products present as cracking products

[d] Binding Energy of oxygen vacancies (O1s) state was characterized by XPS technique.

[e] Amount of total Lewis and Brønsted acid site was investigated by IR spectra of pyridine adsorption (Pyridine-IR)

Among the tested catalysts the most interesting results were obtained for ZrO_2-based catalysts. Table 9 shows that the significant roles of catalytic properties influence catalytic activity and selectivity of this ketonic decarboxylation reaction. Therefore, the catalytic properties can be divided into main two types; (i) the catalytic properties affect the conversion of methyl stearate and (ii) the catalytic properties affect the selectivity of desired ketone product. Besides, the cracking products will be considered in relation to Brønsted acid site causing these undesired products. Apparently, the transition metal oxides ($10\%CeO_2/ZrO_2$, $10\%Y_2O_3/ZrO_2$, and

10%La$_2$O$_3$/ZrO$_2$) group modified ZrO$_2$ catalyst affect the high catalytic activity, great selectivity, and a low content of cracking products. On the other hand, the catalytic performance of this ketonic decarboxylation of methyl stearate over ZrO$_2$ containing alkali metal oxides group (10%MgO/ZrO$_2$ and 10%BaO/ZrO$_2$) catalysts have revealed low conversion, less selectivity, but lots of cracking products. Note that the performance of these two metal oxides group modified ZrO$_2$ catalysts may be related to catalytic activities involving oxygen vacancy (O1s) site, total Lewis acid site, and total Brønsted acid site.

From results above, there are Lewis acid sites as the active sites of 10%CeO$_2$/ZrO$_2$ catalyst more than other catalysts providing the highest conversion of 58.5% % due to CeO$_2$ exhibits strong metal-support interactions [6]. The highest selectivity of main product about 38.7% result from lots of oxygen vacancies sites on catalyst surface, while the lowest of cracking products have occurred since lowest Brønsted acid sites. Simakova, I. L. and Murzin, D. Y.(2016) reported that the incorporation of ceria into ZrO$_2$ [16] was shown to result in an increase of catalytic activity due to absence of an individual CeO$_2$ phase (which has low activity), the formation of solid solution with inter grain boundaries in 10% CeO$_2$/ZrO$_2$ where ZrO$_2$ lattice structure is strongly disordered and exposes highly unsaturated coordination sites, and an increase of total concentration of surface cations [6].

Other metal oxides modified ZrO$_2$ catalyst could be summarized in the same way that if the catalysts have more active site on surface cations in term of Lewis acid sites, they will exhibit the high conversion of methyl stearate. The high content of oxygen vacancy sites couples with low content of Brønsted acid sites on catalytic properties can be also promoted the selectivity [19, 34].

4.4.1 The catalytic properties affect the conversion of methyl stearate.

After matching the catalysts, we found that 10%Y$_2$O$_3$/ZrO$_2$ and 10%La$_2$O$_3$/ZrO$_2$ catalysts already have nice equal conversion close to 50.1% and 50.3%, respectively. The conversion and catalytic properties of each catalyst are shown as follows;

Table 10 Catalytic activity and the properties of 10%Y$_2$O$_3$/ZrO$_2$ and 10%La$_2$O$_3$/ZrO$_2$ catalyst.

Catalysts	Conversion (%)	Binding Energy O1s (eV)	Total Lewis acid site (a.u./g)	Total Brønsted acid site (a.u./g)
10%Y$_2$O$_3$/ZrO$_2$	50.3	4620.12	67.02	4.8
10%La$_2$O$_3$/ZrO$_2$	50.1	2556.76	65.01	7.0

With the total Lewis acid site on the surface of 10%Y$_2$O$_3$/ZrO$_2$ catalyst was detected as equal as on the surface of 10%La$_2$O$_3$/ZrO$_2$ catalyst. From Table 10 can be seen the effect of Lewis acid sites, as active sites, so we can conclude that conversion of methyl stearate only depends on Lewis acid site. And, the oxygen vacancies and Brønsted acid site already have no significant effect on the conversion. On the contrary, Simakova and Murzin (2016) were explained the mechanism of ketonic decarboxylation of carboxylic acid involving two types of active sites; metal cations and oxygen groups when they studied the conversion of pentanoic acid on the test catalysts mainly depends on the total concentration of all types of surface aprotonic acid sites and the concentration of lattice oxygen atoms O^{2-}, which participate in the formation of the intermediate compound [6].

4.4.2 The catalytic properties affect the selectivity of the desired ketone product.

Apparently, ZrO$_2$ and 10%Y$_2$O$_3$/ZrO$_2$ already have similar value of the total Brønsted acid site around 5.1% and 4.8%, respectively. The selectivity and catalytic properties of each catalyst are shown as follows;

Table 11 Selectivity and the properties of ZrO_2 and $10\%Y_2O_3/ZrO_2$ catalyst.

Catalysts	Selectivity (%)	Binding Energy O1s (eV)	Total Brønsted acid site (a.u./g)
ZrO_2	23.5	2665.07	5.1
$10\%Y_2O_3/ZrO_2$	28.4	4620.12	4.8

According to Table 11, the total Brønsted acid site on the surface of ZrO_2 catalyst was similar to the total Brønsted acid site on the surface of $10\%Y_2O_3/ZrO_2$ catalyst. On the other hand, the binding energy of oxygen vacancies (O1s) of ZrO_2 supported catalyst modified with $10\%Y_2O_3$ is higher than pure ZrO_2 catalyst. Therefore, different oxygen vacancies bring to different selectivity. These can be noted that oxygen vacancies (O1s) affect the selectivity of desired ketone product. In the same way, Lili Zhao *et al.* (2019) were studied the synergistic effect of oxygen vacancies and Ni species on tuning selectivity of Ni/ZrO_2 catalyst for hydrogenation of maleic anhydride into succinic anhydride and γ-Butyrolacetone and showed the higher binding energy of the nickel species in the Ni/ZrO_2 further confirmed that nickel species have a stronger interaction with ZrO_2 and can be promoted the selectivity better [35].

Moreover, we focus on the oxygen vacancies of each catalyst for discussing about the effect of Brønsted acid site that also can influence the selectivity of desired ketone product, too.

Table 12 Selectivity and the properties of ZrO_2 and $10\%La_2O_3/ZrO_2$ catalyst.

Catalysts	Selectivity (%)	Binding Energy O1s (eV)	Total Brønsted acid site (a.u./g)
ZrO_2	23.5	2665.07	5.1
$10\%La_2O_3/ZrO_2$	22.0	2556.76	7.0

There is a very similar binding energy of oxygen vacancies (O1s) value of pure ZrO$_2$ supported catalyst and ZrO$_2$ supported catalyst modified with 10%La$_2$O$_3$. The results from Table 12 were displays the 10%Y$_2$O$_3$/ZrO$_2$ catalyst performed lower selectivity than ZrO$_2$ catalyst because of the higher total Brønsted acid site of this modified catalyst. So, Brønsted acid site on the surface of catalyst affecting selectivity as well.

4.4.3 Comparison between oxygen vacancies and Brønsted acid site affect the selectivity of the desired ketone product.

As we have known from Table 11 and Table 12, the selectivity of desired ketone product depends on both of oxygen vacancy and Brønsted acid site. However, one of them can demonstrate a remarkable effect on selectivity. We have described the definition of ratio factors as fractions equaling:

i) $\dfrac{\Delta \text{ Selectivity}}{\Delta \text{ Oxygen Vacancy}}$ = $\dfrac{\dfrac{\text{Maximum - minimum selectivity of ketone product}}{\text{The maximum selectivity of ketone product}}}{\dfrac{\text{Maximum - minimum amount of oxygen vacancy}}{\text{The maximum amount of oxygen vacancy}}}$

ii) $\dfrac{\Delta \text{ Selectivity}}{\Delta \text{ Brønsted acid site}}$ = $\dfrac{\dfrac{\text{Maximum - minimum selectivity of ketone product}}{\text{The maximum selectivity of ketone product}}}{\dfrac{\text{Maximum - minimum amount of Brønsted acid site}}{\text{The maximum amount of Brønsted acid site}}}$

In order to solve this hypothesis, we have to focus on the ratio of selectivity/Brønsted acid site of catalyst, which two pairs of different catalysts. Therefore, (1) ZrO$_2$ and 10%Y$_2$O$_3$/ZrO$_2$ and (2) ZrO$_2$ and 10%La$_2$O$_3$/ZrO$_2$ catalyst will be compared in terms of Δ Selectivity/Δ Oxygen Vacancy and Δ Selectivity/Δ Brønsted acid site, respectively. The results are shown in Table 13, as follows;

Table 13 Comparison between oxygen vacancies and Brønsted acid site affect the selectivity of the desired ketone product.

No.	Catalysts	Selectivity (%)	Binding Energy O1s (eV)	Total Brønsted acid site (a.u./g)	Ratio
1	ZrO_2	23.5	2665.07	5.1	$\mathbf{\Delta}$ Selectivity = 0.41
	10%Y_2O_3/ZrO_2	28.4	4620.12	4.8	$\mathbf{\Delta}$ Oxygen Vacancy
2	ZrO_2	23.5	2665.07	5.1	$\mathbf{\Delta}$ Selectivity = 0.24
	10%La_2O_3/ZrO_2	22.0	2556.76	7.0	$\mathbf{\Delta}$ Brønsted acid site

Importantly, the ratio of selectivity/oxygen vacancy around 0.41, is higher than the ratio of selectivity/Brønsted acid site, 0.24. These can be suggested that higher oxygen vacancy strongly effect to increase ketonic decarboxylation selectivity. That is, the 1 unit of oxygen vacancy site provides higher selectivity than 1 unit of Brønsted acid site. Accordingly, these can be remarked that the oxygen vacancy plays an important role in the selectivity of desired ketone product more than the Brønsted acid site.

จุฬาลงกรณ์มหาวิทยาลัย

CHULALONGKORN UNIVERSITY

CHAPTER V
CONCLUSIONS AND RECOMMENDATIONS

5.1 Conclusions

The 18-pentatriacontanone, high valuable long-chain ketone product, can be produced by via ketonic decarboxylation of methyl stearate over ZrO_2 catalyst at the optimal condition of 400°C and 1 bar. The increasing temperature plays a key role in forming the cracking more than pressure. A loss of selectivity, especially occurring higher reaction temperature, is due to a side reaction of cracking. Then, the metal oxide modified ZrO_2 catalysts were applied for testing at this condition. Almost 58.5% conversion and 38.7% selectivity were achieved, and minimum cracking products were obtained in 0.7%, which has a high content of C35 ketone product more than light fragment cracking of hydrocarbons. It has been found that the catalytic activity of methyl stearate only depends on Lewis acid site as active sites on the surface of catalysts. Moreover, oxygen vacancies and Brønsted acid sites on the surface of catalyst also affecting selectivity as well. Higher oxygen vacancies and lower Brønsted acid sites will promote high selectivity. But this effect has been compared in term of selectivity/ oxygen vacancy or Brønsted acid site ratio, that is, the oxygen vacancy plays an important role in the selectivity of the desired ketone product more than the Brønsted acid site. A detailed understanding of this research is believed to be a prerequisite for the design and development of new improved catalyst systems involving three catalytic properties : (i) high content of Lewis acid sites, (ii) high amount of oxygen vacancies site, and (iii) less Brønsted acid site that can ensure substantial long chain of hydrocarbons, methyl esters, conversion and high desired ketone product selectivity, together with the lowest possible amount of undesired cracking product.

5.2 Recommendations

1) The CaO modified ZrO_2 catalyst should be tested in this reaction for confirming the effect of alkali metal loading for characteristic properties and catalytic performance.

2) Other catalysts with lower Brønsted acid site should be used in ketonic decarboxylation of methyl stearate to minimize cracking products and improve the selectivity of desired ketone product.

3) The study about cracking products occurred from the substrate or main product cracked by using catalyst containing only Brønsted acid on the catalyst surface such as ZSM-5 catalyst.

4) GC-FID condition with the lower initial temperature around 30-40 °C may detect other by-products better. The setup conditions of GC-FID will be important for good analysis.
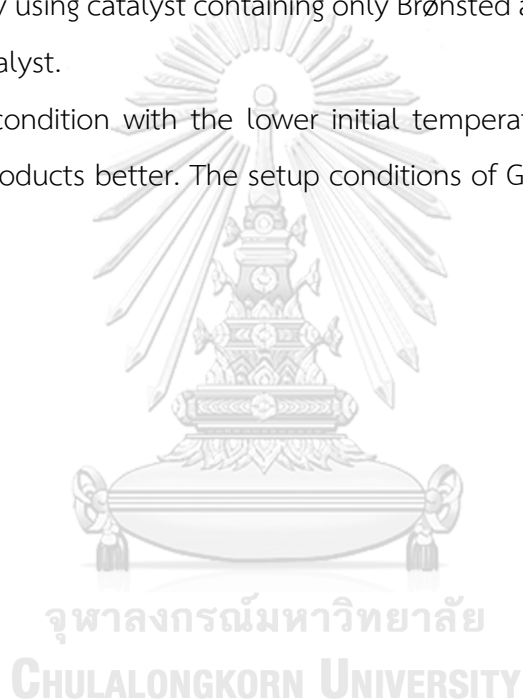
APPENDIX

APPENDIX A

CALCULATION FOR FEED FLOW RATE CONDITION

The recommend flow rate of substrate from experimental part of Borja Oliver-Tomas *et. al.*'s research explained that the substrate was fed at 0.15 mL/min. So, we applied to use this condition in my research [4].

- **Feed flow rate**
    - Methyl stearate (density = 0.8498 g/cm^3)

    Substrate flow rate   = 0.15 mL/min

                                    = 9 mL/h

                                    = 9 mL/h x 0.8498 g/cm^3

                                    = 7.6482 g/h

    - Feed: 10%w/v of methyl stearate diluted in dodecane

    Feed flow rate   = (7.6482 g/h x 100 mL)/10 g

                                    = 76.482 mL/h

                                    = 1.2747 mL/min

- **WSHV**

$$\text{WSHV (h}^{-1}\text{)} = \frac{\text{Feed (kg/h)}}{\text{Mass of catalyst (kg)}}$$

WSHV of substrate   = (9 mL/h x 0.8498 g/mL)/2.5 g of catalyst

                                    = 3.0593 h^{-1}

APPENDIX B

CALCULATION FOR MODIFIED CATALYST PREPARATION

All modified metal oxide catalysts were prepared by incipient wetness impregnation method such as $10\%CeO_2/ZrO_2$, $10\%Y_2O_3/ZrO_2$, $10\%La_2O_3/ZrO_2$, $10\%MgO/ZrO_2$, and $10\%BaO/ZrO_2$.

- **Calculation for the preparation of 10 wt% CeO_2/ZrO_2 catalyst**

Based on 100 g of catalyst used, the composition of catalyst is followed;

ZrO_2 90 g   consisted of Ce metal   = 10 g

ZrO_2 3 g   consisted of Ce metal   = 0.3333 g_{Ce}

Precursor: Cerium (III) nitrate hexahydrate 99% ($CeN_3O_9.6H_2O$)

Precursor 434.22 g_{Pre} → Ce metal = 1x0.99x140.116 = 138.7148 g_{Ce}

Precursor is required for (0.3333 g_{Ce}x434.22 g_{Pre})/138.7148 g_{Ce} = 1.0433 g_{Pre}

- **Calculation for the preparation of 10 wt% Y_2O_3/ZrO_2 catalyst**

Based on 100 g of catalyst used, the composition of catalyst is followed;

ZrO_2 90 g   consisted of Y metal   = 10 g

ZrO_2 3 g   consisted of Y metal   = 0.3333 g_Y

Precursor: Yttrium (III) nitrate hexahydrate 99.9% ($YN_3O_9.6H_2O$)

Precursor 383.01 g_{Pre} → Y metal = 1x0.999x88.91 = 88.8211 g_Y

Precursor is required for (0.3333 g_Yx383.01 g_{Pre})/88.8211 g_Y = 1.4372 g_{Pre}

- **Calculation for the preparation of 10 wt% La_2O_3/ZrO_2 catalyst**

Based on 100 g of catalyst used, the composition of catalyst is followed;

ZrO_2 90 g   consisted of La metal   = 10 g

ZrO_2 3 g   consisted of La metal   = 0.3333 g_{La}

Precursor: Lanthanum (III) nitrate hexahydrate 99.9% ($LaN_3O_9.6H_2O$)

Precursor 433.01 g_{Pre} → La metal = 1x0.999x138.905 = 138.7661 g_{La}

Precursor is required for (0.3333 g_{La}x433.01 g_{Pre})/ 138.7661 g_{La} = 1.0400 g_{Pre}

- **Calculation for the preparation of 10 wt% MgO/ZrO$_2$ catalyst**

Based on 100 g of catalyst used, the composition of catalyst is followed;

ZrO$_2$ 90 g   consisted of Mg metal   = 10 g

ZrO$_2$ 3 g   consisted of Mg metal   = 0.3333 g_{Mg}

<u>Precursor</u>: Magnesium nitrate hexahydrate 99% (MgN$_2$O$_6$.6H$_2$O)

Precursor 256.41 g_{Pre} → Mg metal = 1x0.99x24.305 = 88.8211 g_{Mg}

Precursor is required for (0.3333 g_{Mg}x256.41 g_{Pre})/24.0619 g_{Mg} = 3.5517 g_{Pre}

- **Calculation for the preparation of 10 wt% BaO/ZrO$_2$ catalyst**

Based on 100 g of catalyst used, the composition of catalyst is followed;

ZrO$_2$ 90 g   consisted of Ba metal   = 10 g

ZrO$_2$ 3 g   consisted of Ba metal   = 0.3333 g_{Ba}

<u>Precursor</u>: Barium chloride 99.9% (BaCl$_2$.2H$_2$O)

Precursor 244.27 g_{Pre} → Ba metal = 1x0.999x137.327 = 137.1897 g_{Ba}

Precursor is required for (0.3333 g_{Ba}x244.27 g_{Pre})/137.1897 g_{Ba} = 0.5934 g_{Pre}

- **Calculation for the preparation of 5 wt% La$_2$O$_3$/ZrO$_2$ catalyst**

Based on 100 g of catalyst used, the composition of catalyst is followed;

ZrO$_2$ 95 g   consisted of La metal   = 5 g

ZrO$_2$ 3 g   consisted of La metal   = 0.1579 g_{La}

<u>Precursor</u>: Lanthanum (III) nitrate hexahydrate 99.9% (LaN$_3$O$_9$.6H$_2$O)

Precursor 433.01 g_{Pre} → La metal = 1x0.999x138.905 = 138.7661 g_{La}

Precursor is required for (0.1579 g_{La}x433.01 g_{Pre})/138.7661 g_{La} = 0.4927 g_{Pre}

APPENDIX C

CHARACTERIZATION

- **SEM-EDX**

The elemental analysis was investigated by SEM-EDX technique which the result was summarized in Table 13.

Table 14 The elemental analysis of ZrO_2 and metal oxide modified ZrO_2 catalysts. was investigated by SEM-EDX technique.

Sample	Element	Wt%	At%
ZrO_2	OK	27.51	68.39
	ZrL	72.49	31.61
$10\%CeO_2/ZrO_2$	CeL	10.72	3.65
$10\%Y_2O_3/ZrO_2$	YL	9.72	3.68
$10\%La_2O_3/ZrO_2$	LaL	9.74	3.27
$10\%MgO/ZrO_2$	MgK	10.99	16.60
$10\%BaO/ZrO_2$	BaqL	10.94	3.23
$5\%La_2O_3/ZrO_2$	LaL	05.11	01.80

- N$_2$-Physisorption

$$\text{Surface area (m}^2\text{g}^{-1}\text{)} = \frac{\text{Nitrogen desorption (m}^2\text{)}}{\text{Mass of sample (g)}}$$

Table 15 The surface area of ZrO$_2$ and metal oxide modified ZrO$_2$ catalysts was characterized by N$_2$-Physisorption.

Sample	Mass of sample (g)	Nitrogen desorption (m^2)	Surface area (m^{2}g^{-1})
ZrO$_2$	0.0592	5.425	91.6
10%CeO$_2$/ZrO$_2$	0.0601	4.55	75.7
10%Y$_2$O$_3$/ZrO$_2$	0.0597	2.835	47.5
10%La$_2$O$_3$/ZrO$_2$	0.0598	2.415	40.4
10%MgO/ZrO$_2$	0.0597	2.52	42.2
10%BaO/ZrO$_2$	0.0590	1.96	33.2
5%La$_2$O$_3$/ZrO$_2$	0.0588	4.07	69.3

จุฬาลงกรณ์มหาวิทยาลัย

CHULALONGKORN UNIVERSITY

● IR spectra of pyridine adsorption (Py-IR)

Total Lewis or Brønsted acid = <u>Area of Py-Adsorption</u>

(a.u./$g_{catalyst}$)　　　　Mass of sample (g)

Table 16 Surface acidity of ZrO_2 and metal oxide modified ZrO_2 catalysts.

Sample	Mass of sample (g)	Wavenumbers (cm^{-1})	Area of pyridine adsorption	Total Lewis acid (a.u./g)	Total Brønsted acid (a.u./g)
ZrO_2	0.0324	1442.54	1.7020	52.53	7.00
		1539.88	0.2268		
10%CeO_2/ZrO_2	0.0312	1440.22	2.7050	86.70	2.10
		1540.51	0.0655		
10%Y_2O_3/ZrO_2	0.0334	1441.13	2.2386	67.02	4.80
		1540.52	0.1603		
10%La_2O_3/ZrO_2	0.0473	1440.05	3.0750	65.01	5.10
		1541.19	0.2412		
10%MgO/ZrO_2	0.0315	1440.70	1.0487	33.29	8.50
		1539.90	0.2678		
10%BaO/ZrO_2	0.0342	1440.66	0.6065	17.73	23.90
		1539.33	0.8174		
5%La_2O_3/ZrO_2	0.0326	1440.68	0.9324	28.6	3.80
		1541.17	0.1239		

APPENDIX D

CALCULTION CONVERSION AND SELECTIVITY

Catalytic activity for substrate, methyl stearate, and 18-pentatriacontanone were evaluated by moles from the calibration curve versus area from GC-FID analysis.

- **Calibration curve of methyl stearate**

Figure 27 Calibration curve of methyl stearate
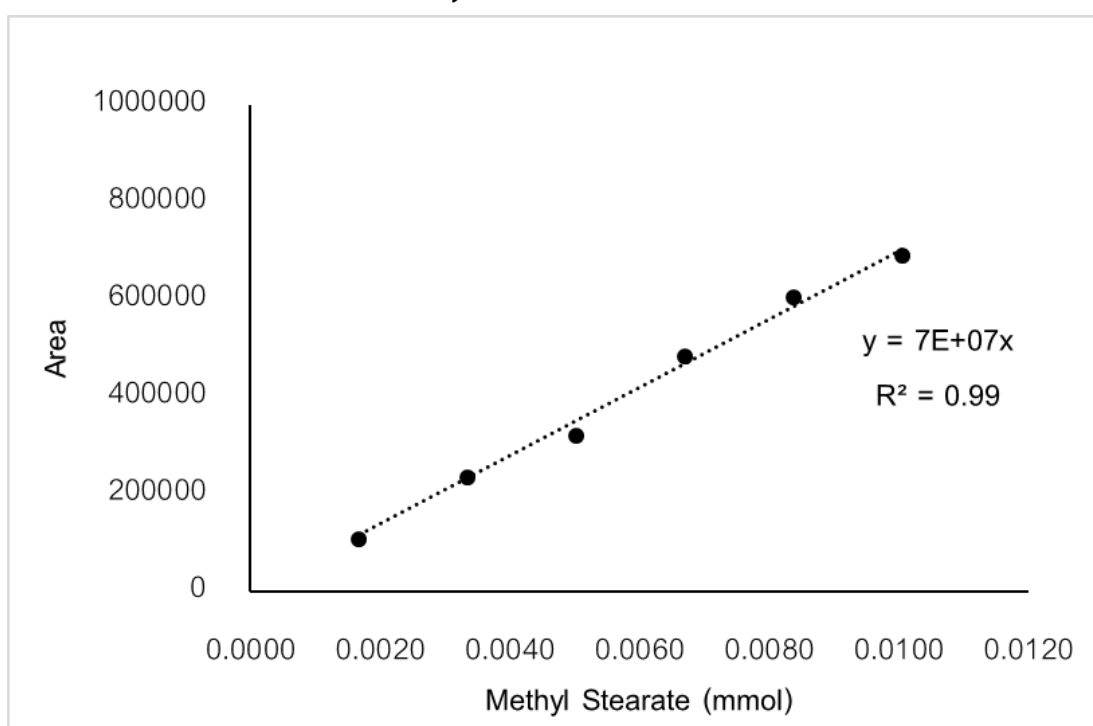
- Calibration curve of 18-pentatriacontanone
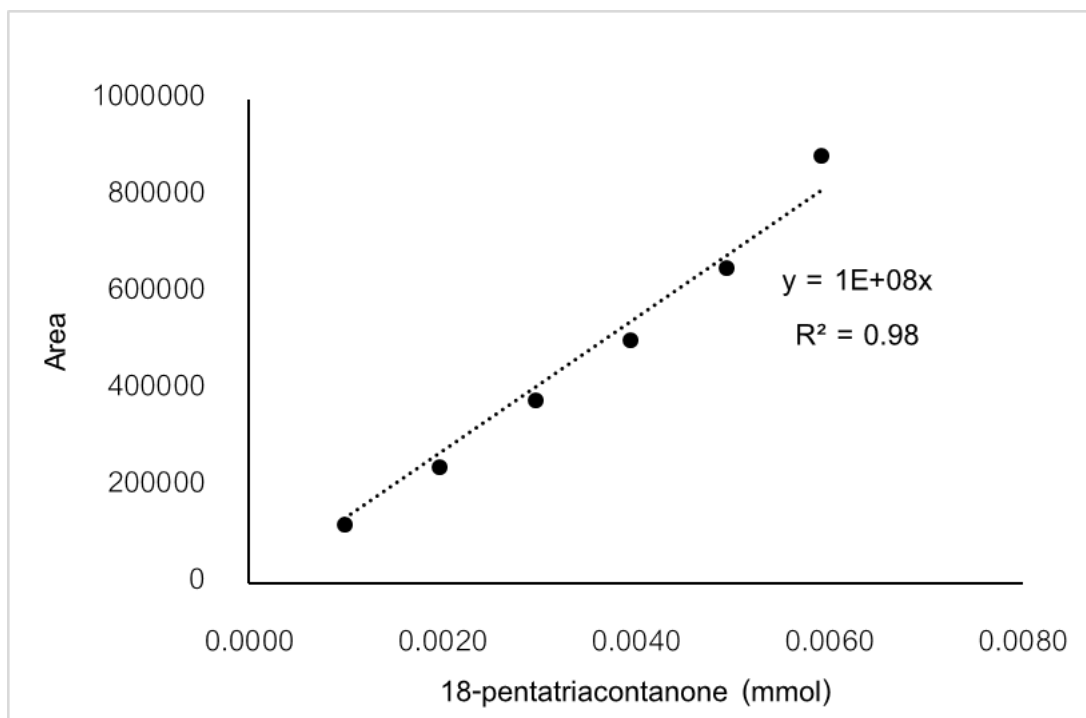
Figure 28 Calibration curve of 18-pentatriacontanone

- Determination of percent of conversion of methyl stearate and selectivity to 18-pentatriacontanone.

$$\%Conversion = \frac{Mole_{MS,in} - Mole_{MS,out}}{Mole_{MS,in}}$$

Mole $_{MS,\,in}$ is mole of methyl stearate inlet

Mole $_{MS,\,out}$ is mole of methyl stearate outlet

$$\%\text{Selectivity} = \frac{Mole_{C35,out}}{Mole_{MS,in} - Mole_{MS,out}}$$

Mole $_{C35, out}$ is mole of 18-pentatriacontanone (C35) outlet

Mole $_{MS, in}$ is mole of methyl stearate inlet

Mole $_{MS, out}$ is mole of methyl stearate outlet

$$\%\text{Cracking} = \frac{Area_{cracking,out}}{Area_{MS,in} - Area_{MS,out}}$$

Area $_{cracking, out}$ is area of cracking product outlet

Area $_{MS, in}$ is area of methyl stearate inlet

Area $_{MS, out}$ is area of methyl stearate outlet

จุฬาลงกรณ์มหาวิทยาลัย

CHULALONGKORN UNIVERSITY

REFERENCES

1. Patil, P.D. and S. Deng, *Optimization of biodiesel production from edible and non-edible vegetable oils.* Fuel, 2009. **88**(7): p. 1302-1306.

2. Leung, D.Y.C., X. Wu, and M.K.H. Leung, *A review on biodiesel production using catalyzed transesterification.* Applied Energy, 2010. **87**(4): p. 1083-1095.

3. Raksaseri, K. *THAILAND: Firm on Protecting the Palm Oil Sector*. 2015 [cited 2019; Available from: http://www.aseannews.net/thailand-firm-protecting-palm-oil-sector/.

4. Oliver-Tomas, B., M. Renz, and A. Corma, *High Quality Biowaxes from Fatty Acids and Fatty Esters: Catalyst and Reaction Mechanism for Accompanying Reactions.* Industrial & Engineering Chemistry Research, 2017. **56**(45): p. 12870-12877.

5. Ramos, M.J., et al., *Influence of fatty acid composition of raw materials on biodiesel properties*. Vol. 100. 2008. 261-8.

6. Simakova, I.L. and D.Y. Murzin, *Transformation of bio-derived acids into fuel-like alkanes via ketonic decarboxylation and hydrodeoxygenation: Design of multifunctional catalyst, kinetic and mechanistic aspects.* Journal of Energy Chemistry, 2016. **25**(2): p. 208-224.

7. Oliver-Tomas, B., et al., *Effect of the Cα substitution on the ketonic decarboxylation of carboxylic acids over m-ZrO2: the role of entropy.* Catalysis Science & Technology, 2016. **6**(14): p. 5561-5566.

8. Pulido, A., et al., *Ketonic Decarboxylation Reaction Mechanism: A Combined Experimental and DFT Study.* ChemSusChem, 2013. **6**(1): p. 141-151.

9. PubChem. *Methyl Stearate*. [cited 2019; Available from: https://pubchem.ncbi.nlm.nih.gov/compound/methyl_stearate.

10. ChemicalBook. *METHYL STEARATE*. [cited 2019; Available from: https://www.chemicalbook.com/ChemicalProductProperty_EN_CB6409834.htm.

11. PubChem. *18-Pentatriacontanone*. [cited 2019; Available from: https://pubchem.ncbi.nlm.nih.gov/compound/18-pentatriacontanone.

12. Scientific, A.A.b.T.F. *18-Pentatriacontanone, tech. 85%* [cited 2019; Available from: https://www.alfa.com/en/catalog/041445/.

13. Rothman, E.S., *PROCESS FOR THE PREPARATION OF STEARONE* U.S.P. Office, Editor. 1966: United States of America

14. Renz, M., *Ketonization of Carboxylic Acids by Decarboxylation: Mechanism and Scope.* European Journal of Organic Chemistry, 2005. **2005**(6): p. 979-988.

15. Pham, T.N., et al., *Ketonization of Carboxylic Acids: Mechanisms, Catalysts, and Implications for Biomass Conversion.* ACS Catalysis, 2013. **3**(11): p. 2456-2473.

16. Zaytseva, Y.A., et al., *Effect of Gas Atmosphere on Catalytic Behaviour of Zirconia, Ceria and Ceria–Zirconia Catalysts in Valeric Acid Ketonization.* Topics in Catalysis, 2013. **56**(9): p. 846-855.

17. Liang, S.I.H.A.J.-B., *PROCESS FOR PRODUCING KETONES FROM FATTYACIDS* 2013, Chevron U.S.A. Inc.: USA. p. 1-7.

18. Roman Klimkiewicza, Helena Teteryczb, Hanna Grabowskaa, Ireneusz Morawskic, Ludwik Syperb, and Benedykt W. Licznerskib, *Ketonization of Fatty Methyl Esters over Sn-Ce-Rh-O Catalyst* JAOCS, 2001. **Vol. 78**(no. 5).

19. Abbot, J., *Role of Brønsted and Lewis acid sites during cracking reactions of alkanes.* Applied Catalysis, 1989. **47**(1): p. 33-44.

20. Kissin, Y.V., *CHEMICAL MECHANISMS OF CATALYTIC CRACKING OVER SOLID ACIDIC CATALYSTS: ALKANES AND ALKENES.* Catalysis Reviews, 2001. **43**(1-2): p. 85-146.

21. Pacchioni, G., *Ketonization of Carboxylic Acids in Biomass Conversion over TiO2 and ZrO2 Surfaces: A DFT Perspective.* ACS Catalysis, 2014. **4**(9): p. 2874-2888.

22. Gliński, M., et al., *Catalytic ketonization over metal oxide catalysts. XIII. Comparative measurements of activity of oxides of 32 chemical elements in ketonization of propanoic acid.* Applied Catalysis A: General, 2014. **470**: p. 278-284.

23. Puigdollers, A.R., F. Illas, and G. Pacchioni, *Structure and Properties of Zirconia Nanoparticles from Density Functional Theory Calculations.* The Journal of Physical Chemistry C, 2016. **120**(8): p. 4392-4402.

24. Gliński, M., J. Kijeński, and A. Jakubowski, *Ketones from monocarboxylic acids: Catalytic ketonization over oxide systems.* Applied Catalysis A: General, 1995. **128**(2): p. 209-217.

25. A. G. Gasanov, A.G.A., S. T. Aliyeva, G. D. Gasanova, and S.R.K. N. S. Guseynov, I. G. Ayyubov, *APPLICATION OF MAGNESIUM AND TITANIUM OXIDES AS CATALYSTS IN REACTION DECARBOXYLATION OF ACIDS.* Processes of petrochemistry and oil-refining, 2013. **14**(3(55)): p. 169-174.

26. Shutilov, A.A., et al., *Phase composition and catalytic properties of ZrO2 and CeO2-ZrO2 in the ketonization of pentanoic acid to 5-nonanone.* Kinetics and Catalysis, 2013. **54**(2): p. 184-192.

27. Camacho, D.M., et al., *Solubility and Nucleation of Methyl Stearate as a Function of Crystallization Environment.* Energy & Fuels, 2018. **32**(3): p. 3447-3459.

28. Campbell, J.A., *Le Châtelier's principle, temperature effects, and entropy.* Journal of Chemical Education, 1985. **62**(3): p. 231.

29. Sakata, Y., et al., *Preparation of a New Type of CaSiO3 with High Surface Area and Property as a Catalyst Support,* in *Studies in Surface Science and Catalysis,* E.M. Gaigneaux, et al., Editors. 2006, Elsevier. p. 331-338.

30. E, K., P. Selvarajan, and D. Muthuraj, *Synthesis and Characterization of CeO2 Nanocrystals by Solvothermal Route.* Vol. 16. 2013. 269-276.

31. Jun, J., et al., *Surface properties and photoactivity of TiO2 treated with electron beam.* Radiation Physics and Chemistry, 2006. **75**(5): p. 583-589.

32. Sinhamahapatra, A., et al., *Oxygen-Deficient Zirconia (ZrO2-x): A New Material for Solar Light Absorption.* Scientific reports, 2016. **6**: p. 27218-27218.

33. Zhu, S., et al., *Hydrogenolysis of glycerol to 1,3-propanediol over bifunctional catalysts containing Pt and heteropolyacids.* Catalysis Today, 2013. **212**: p. 120-126.

34. Wu, G.-S., et al., *Implication of the role of oxygen anions and oxygen vacancies for methanol decomposition over zirconia supported copper catalysts.* Vol. 253. 2006. 974-982.

35.   Zhao, L., et al., *Synergistic Effect of Oxygen Vacancies and Ni Species on Tuning Selectivity of Ni/ZrO2 Catalyst for Hydrogenation of Maleic Anhydride into Succinic Anhydride and **γ**-Butyrolacetone*. Vol. 9. 2019. 406.

VITA

NAME   Pawaphat Sartsri

DATE OF BIRTH   14 December 1994

PLACE OF BIRTH   Chainat, Thailand

INSTITUTIONS ATTENDED   2013 - Graduated high school from Chainatpittayakom
                                School.
                                2017 - Graduated Bachelor's Degrees from Faculty of
                                Engineering in Chemical Engineering, King Mongkut's
                                Institute of Technology Ladkrabang, Bangkok, Thailand.

HOME ADDRESS   119/16 Tessaban 6 Alley, Bankluay Sub-district, Mueang
                                Chai Nat,
                                Chai Nat, 17000, Thailand